A Project on

Soft Robotic Gripper Using NiTi Coils

Submitted for fulfilment of award of

Bachelor of Technology

In

Electrical and Electronics

By

Raghvendra Singh
Shubham Gupta
Utkarsh Rastogi

Under the Guidance of

Vikash Kumar
Rahul Dixit

AJAY KUMAR GARG ENGINEERING COLLEGE, GHAZIABAD
YEAR: 2015-2016

AJAY KUMAR GARG ENGINEERING COLLEGE, GHAZIABAD

CERTIFICATE

This is to certify that Project Report entitled "SOFT ROBOTIC GRIPPER USING NiTi COILS" which is submitted by Raghvendra Singh, Shubham Gupta and Utkarsh Rastogi in the partial fulfillment of requirement for the award of degree of Bachelor of Technology (Electrical and Electronic Engineering) submitted to A.P.J Abdul Kalam Technical University, Lucknow is a record of students' own work carried out under my supervision. The matter in this report has not been submitted to any University or Institution for award of any degree.

Supervisors:
Vikash Kumar
Rahul Dixit

HOD:
Prof. Ashiv Shah
TIFAC CORE

Date: 29th April, 2016.

ACKNOWLEDGEMENT

We take this opportunity to express our deep sense of gratitude and regard to **Mr. Vikash Kumar** (TIFAC CORE Deptt.) and **Mr. Rahul Dixit** (TIFAC CORE Deptt.), Ajay Kumar Garg Engineering College, Ghaziabad for his continuous encouragement and able guidance, we needed to complete this project.

We would pay sincere gratitude to the Head of the Deptt. (TIFAC CORE) Prof. Ashiv Shah for his precious and enlightening words of wisdom which motivated us throughout our project work.

We are also grateful to **Mr. Ashish Gupta** and **Mr. Harikesh Bahadur Singh** for their continuous support and valuable suggestions.

DECLARATION

We hereby declare that this submission is our own work and that, to the best of out knowledge and belief, it contains no material previously published or written by another person, nor material which to a substantial extent has been accepted for the award of any other degree or diploma by the university or other institute of higher learning, except where due acknowledgement has been made in the text.

Signature:

1.

Name: Shubham Gupta

Roll No. : 1202721090

2.

Name: Raghvendra Singh

Roll No. : 1202721065

3.

Name: Utkarsh Rastogi

Roll No. : 1202731109

TABLE OF CONTENTS

LIST OF FIGURES

ABSTRACT

Robotics is basically based on the fundamental assumption that robots are chain of rigid links but 'Soft Robotics' which is the use of soft materials in robotics that can vary their stiffness and thus can undergo high deformations during interactions that overcomes robot's basic assumptions and thus removes many bottlenecks of rigid links in robots. They can have mechanisms for varying the material characteristics such as stiffness, elasticity and surface properties, etc. for generating motion through muscles and for facilitating sensing in skins through embedded mechanoreceptors. Soft materials may enable us to automate tasks that are beyond capacities of current robotics technology and thus the complex, precise control architecture can be simplified using highly compliant materials with variable stiffness. Soft Robots has the expected capability to interact more easily and effectively with the real world environment. Soft Robotics has the potential to produce a new generation of better robots.

This report presents the development and analysis of a soft robotic platform that exhibits the grasping and release action of a human hand. The design of the gripper is basically based on a human hand except for the fact that all the joint to joint distances in a finger are equal. Each finger is composed of four sub-components and three fingers are joint together to a base to form the hand. Nickel titanium (NiTi) coils are used as the actuating medium and are placed across the joints of the finger. The finger sub-components are made of PLA using a 3D printer. The actuation of the nickel titanium coils is controlled through a constant current supply, controlled through a switching circuit and a microcontroller. This approach allows for a simple, low cost, energy efficient gripper. The report further analysis and discusses the potential use and application of this platform.

***Index Terms*—Robotic gripper, nickel titanium (NiTi) coil actuators, PLA, soft robotics, shape memory alloys (SMA) actuation, microcontroller, 3D printer.**

Chapter 1.
INTRODUCTION

1.1 Robot End Effectors

In robotics, an end effector is the device at the end of a robotic arm, designed to interact with the environment. The exact nature of this device depends on the application of the robot. In the strict definition, which originates from serial robotic manipulators, the end effector means the last link (or end) of the robot. At this endpoint the tools are attached. In a wider sense, an end effector can be seen as the part of a robot that interacts with the work environment. This does not refer to the wheels of a mobile robot or the feet of a humanoid robot which are also not end effectors—they are part of the robot's mobility.

End effectors may consist of a gripper or a tool. When referring to robotic prehension there are four general categories of robot grippers, these are: [1]

a) Impactive – jaws or claws which physically grasp by direct impact upon the object.
b) Ingressive – pins, needles or hackles which physically penetrate the surface of the object (used in textile, carbon and glass fibre handling).
c) Astrictive – suction forces applied to the objects surface (whether by vacuum, magneto or electro adhesion).
d) Contigutive – requiring direct contact for adhesion to take place (such as glue, surface tension or freezing).

They are based on different physical effects used to guarantee a stable grasping between a gripper and the object to be grasped.[2] Industrial grippers can be mechanical, the most diffused in industry, but also based on suction or on the magnetic force. Vacuum cups and electromagnets dominate the automotive field and in particular metal sheet handling. Bernoulli grippers exploit the airflow between the gripper and the part that causes a lifting force which brings the gripper and part close each other (i.e. the Bernoulli's principle). Bernoulli grippers are a type of contactless grippers, namely the object remains confined in the force field generated by the gripper without coming into direct contact with it. Bernoulli grippers have been adopted in photovoltaic cell handling, silicon wafer handling, and also in the textile and leather industries. Other principles are less used at the macro scale (part size >5mm), but in the last ten years they demonstrated interesting applications in micro handling. Some of them are ready of spreading out their original field. The other adopted principles are: Electrostatic grippers and van der Waals grippers based on electrostatic charges (i.e. van der Waals' force), capillary grippers and cryogenic grippers, based on liquid medium, and ultrasonic grippers and laser grippers, two contactless grasping principles. Electrostatic grippers are based on charge difference between the gripper and the part (i.e. electrostatic force) often activated by the gripper itself, while van der Waals grippers are based on the low force (still electrostatic) due to the atomic attraction between the molecules of the gripper and those of the object.

Capillary grippers use the surface tension of a liquid meniscus between the gripper and the part to center, align and grasp the part, cryogenic grippers freeze a small amount of liquid and the resulting ice guarantees the necessary force to lift and handle the object (this principle is used also in food handling and in textile grasping). Even more complex are ultrasonic based grippers, where pressure standing waves are used to lift up a part and trap it at a certain level (example of levitation are both at the micro level, in screw and gasket handling, and at the macro scale, in solar cell or silicon wafer handling), and laser

source that produces a pressure able to trap and move micro parts in a liquid medium (mainly cells). The laser gripper are known also as laser tweezers.

A particular category of friction/jaw gripper are the needle grippers: they are called intrusive grippers and exploits both friction and form closure as standard mechanical grippers. The most known grippers can be of two, three or even five fingers. The end effectors that can be used as tools serve various purposes, such as spot welding in an assembly, spray painting where uniformity of painting is necessary, and for other purposes where the working conditions are dangerous for human beings. Surgical robots have end effectors that are specifically manufactured for the purpose.

1.2 *Biologically Inspired Engineering*

[3] Biologically inspired engineering is a new scientific discipline that applies biological principles to develop new engineering solutions for medicine, industry, the environment, and many other fields that have previously not been touched by the biology revolution. The emergence of this new discipline is the culmination of the unification of the life sciences with engineering and the physical sciences, and it is leading to an ever deeper understanding of how life works. Biologically inspired engineering involves deep exploration into the way that living cells, tissues, and organisms build, control, manufacture, recycle, and adapt to their environment. Bioinspired engineers leverage this knowledge to innovate new technologies and translate them into products that meet real world challenges.

Biologically inspired engineering is an interdisciplinary field encompassing many specialty areas in biology (molecular cell biology, genetic engineering, developmental biology, organismal biology, clinical medicine), engineering (biomedical engineering, chemical engineering, mechanical engineering, electrical engineering, robotics), and the physical sciences (chemistry, physics, materials science, and nanotechnology). Integrated research programs in this area span many of these disciplines and include biomimicry, as well as analysis of the way that living systems form and function using self-assembling nanomaterials, complex dynamic networks, nonlinear dynamical control, self-organizing behaviour, evolution, and natural selection.

1.2.1 Bio-inspired Robotics

Bio-inspired robotic locomotion is a fairly new sub-category of bio-inspired design. It is about learning concepts from nature and applying them to the design of real world engineered systems. More specifically, this field is about making robots that are inspired by biological systems. Biomimicry and bio-inspired design are sometimes confused. Biomimicry is copying the nature while bio-inspired design is learning from nature and making a mechanism that is simpler and more effective than the system observed in nature. Biomimicry has led to the development of a different branch of robotics called soft robotics. The biological systems have been optimized for specific tasks according to their habitat. However, they are multi-functional and are not designed for only one specific functionality.

Bio-inspired robotics is about studying biological systems, and look for the mechanisms that may solve a problem in the engineering field. The designer should then try to simplify and enhance that mechanism for the specific task of interest. Bio-inspired roboticists are usually interested in biosensors (e.g. eye), bio actuators (e.g. muscle), or

biomaterials (e.g. spider silk). Most of the robots have some type of locomotion system. Thus, in this article different modes of animal locomotion and few examples of the corresponding bio-inspired robots are introduced.

1.2.1.1 Soft Robotics

Soft robotics [4] is a new field in robotics and the idea is to make all of the components in the robot soft and flexible in order to move in very limited spaces and change gaits fairly easily. This field is inspired by animals such as octopus or starfish. One of the first multigait soft robots is developed at Harvard University and is inspired by starfish. [5] Soft robotics is not just a new direction of technological development, but a novel approach to robotics, unhinging its fundamentals, with the potential to produce a new generation of robots, in the support of humans in our natural environments.

1.3 *Mechanism of Gripping*

A common form of robotic grasping is force closure. [6] Generally, the gripping mechanism is done by the grippers or mechanical fingers. Generally only two finger grippers are used for industrial robots as they tend to be built for specific tasks and can therefore be less complex.
The fingers are also replaceable whether or not the gripper itself is replaced. There are two mechanisms of gripping the object in between the fingers (for the sake of simplicity, the following explanations consider only two finger grippers).

1.3.1 *Shape of the gripping surface*

The shape of the gripping surface of the fingers can be chosen according to the shape of the objects that are to be manipulated. For example, if a robot is designed to lift a round object, the gripper surface shape can be a concave impression of it to make the grip efficient, or for a square shape the surface can be a plane.

1.3.2 *Force required to grip the object*

Though there are numerous forces acting over the body that has been lifted by the robotic arm, the main force acting there is the frictional force. The gripping surface can be made of a soft material with high coefficient of friction so that the surface of the object is not damaged. The robotic gripper must withstand not only the weight of the object but also acceleration and the motion that is caused due to frequent movement of the object. To find out the force required to grip the object, the following formula is used:

$$F = \mu W n$$

Where:

F is the force required to grip the object,
μ is the coefficient of friction,
n is the number of fingers in the gripper and
W is the weight of the object.

But the above equation is incomplete. The direction of the movement also plays an important role over the gripping of the object. For example, when the body is moved upwards, against the gravitational force, the force required will be more than towards the gravitational force. Hence, another term is introduced and the formula becomes:

$$F = \mu W n g$$

Here, the value of g should not be taken as the acceleration due to gravity. In fact, here g stands for multiplication factor. The value of g ranges from 1 to 3. When the body is moved in the horizontal direction then the value is taken to be 2, when moved against the gravitational force then 3 and along the gravitational force, i.e., downwards, 1.

1.4 *Examples of End effectors*

The end effector of an assembly line robot would typically be a welding head, or a paint spray gun. A surgical robot's end effector could be a scalpel or others tools used in surgery. Other possible end effectors are machine tools, like a drill or milling cutters. The end effector on the space shuttle's robotic arm uses a pattern of wires which close like the aperture of a camera around a handle or other grasping point.

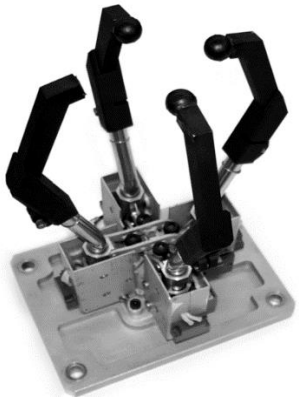

(a.)

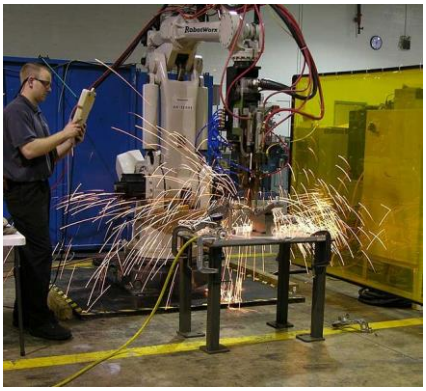

(b.)

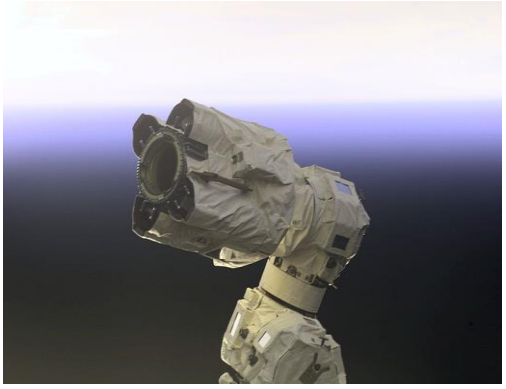

(c.)

(d.)

(e)

Fig. 1.1 (a.) An example of a basic force-closure end effector. (b.) A spot welding end effector. (c.) A repair and observation end effector in use in space (Canadarm2). (d.) A highly sophisticated attempt at reproducing the human-hand force-closure end effector. (e.) Laser Welding end effector.

Chapter 2.
LITERATURE REVIEW, REQUIREMENT ANALYSIS & FEASIBILITY

2.1 Literature Review

[7] Soft robotics is an emerging field that introduces a number of new challenges to roboticists. Soft robots will consist of a flexible body, possess an ability to deform their shape as dictated by various environments, and exhibit superb robustness upon impacts. One of the most challenging elements of such a robot is the soft actuator. Most conventional actuators contain rigid components that limit morphing ability, however a soft actuator can deform along with the surrounding structure.

One of these soft actuators is Nickel Titanium (NiTi) a Shape Memory Alloy (SMA), since its unique martensite transformation makes it inherently flexible. It is also well known for its high energy density, despite its poor efficiency. NiTi has great advantages especially in a small scale where other types of actuators are not available or exhibit poor energy density. The NiTi crystal lattice transforms from the martensite state to the austenite state and produces up to 4% length change as it is heated through the transition temperature range. Some applications require more operating strain to satisfy the dimensional constraints. In order to create larger stroke lengths out of a small lattice structure alteration, NiTi can be restructured into coil springs.

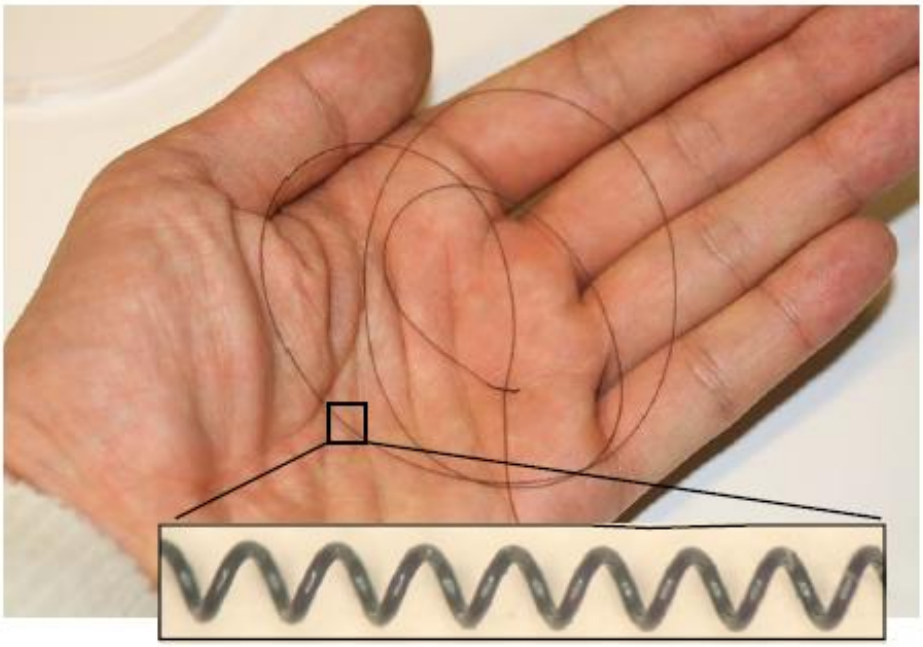

Fig. 2.1 Fabricated muscle fiber is 400μm in diameter and 0.5m

Chang et al. [8], discuss the numerous models for NiTi that has been proposed since the early 1990s. Most of them are thermodynamic models of NiTi wires, tubes, and sheets. Some papers discuss NiTi springs [9], [10], [11], [12], [13], but the models used in these papers are not complete. The paper [7], presents a more complete model that can be used as a design guideline for NiTi spring actuators.

NiTi coil springs are created from straight wire wound into a coil shape and annealed at a high temperature to reset the 'memorized' shape. The annealing temperature used in the reshaping process affects mechanical properties of NiTi and actuation performance. The results from experiments to show the variation in properties due to the variation in annealing temperature have also been presented. These experiments include detwinning force and loaded displacement measurements. After weightlifting test, springs shows permanent deformation, which is also function of the annealing temperature.

2.1.1 NiTi Coil Actuators as Micro Artificial Muscle Fibers

NiTi is one of the well-known SMA materials that generate mechanical work by phase change. Despite its low efficiency, it has a high energy density, which gives the ability to develop relatively small scale actuators compared to other types of actuators mentioned in Section I. In a solid state phase transformation, the crystal structure of the NiTi compound transforms from martensite to austenite states with up to 7% strain change [14]. For larger displacements, coiled spring NiTi wires can be used.

Various NiTi models suggested from the 1990s are discussed in [15]. These are mostly thermodynamic models of various forms of NiTi such as wires, tubes, and sheets. Coiled spring NiTi models were discussed in [9], and [10]–[12]. These models, however, are relatively incomplete. The existing models focus on the mechanical coiled spring equations using different shear moduli for the martensite and austenite phases, overlooking the change in the free length of the spring due to the phase transition.

A more appropriate model, which is useful for a design of coiled spring NiTi is proposed in Section 2.1.2. This model combines the mechanical and thermodynamic aspects of NiTi coil actuators to describe the overall martensite deformation and the geometrical spring effect together. We use this model as a guideline for actuator design for the Meshworm robot.

There are two major steps to fabricate NiTi coil springs. First, a NiTi wire is wound around a straight core, and then the coiled NiTi wire is annealed at a certain high temperature in order to reset the memorized shape as a spring. During the annealing process, mechanical properties and the actuation performance of NiTi springs are determined by the annealing temperature. In Chapter 2.1.2, the manufacturing process is detailed and experimental data between deflection and force under various annealing temperatures are presented.

2.1.2 Modelling of NiTi Coil Actuators

Even though NiTi spring actuators are widely used [9], [10]–[12], complete design models have not been developed yet. Recent works utilize the mechanical coiled spring equation with two shear moduli, $G_M$and G_A which are the martensite and austenite phases, respectively. However, none of these models consider the free length change of the NiTi spring due to phase change. The free length of 100% austenite phase x_{Ao} is shorter than the free length of 100% martensite x_{Mo}.

There are two major physical phenomena in NiTi coil spring deformation. One is the free length change due to the phase transformation explained earlier, and the other is the spring constant difference between the martensite and austenite states. The spring constant in the austenite phase is around 2–3 times greater than in the martensite phase [15].

[16] Fig. 2.2 shows five typical states of a NiTi coil spring during actuation. When the NiTi coil is heated up above the phase transition temperature, it becomes austenite and fully contracts as in Fig. 2.2(a). If a load F is applied in this state, the spring will have a displacement δ_H as shown in Fig. 2.2(b). When the temperature is below the transition temperature, it becomes martensite and the crystal structure of NiTi twins [17] without an observable overall shape change [see Fig. 2.2(c)]. If a load is applied below the transition temperature, the crystal structure is detwinned [17]. Fig. 2.2(e) shows the detwinned martensite with a load F, and Fig. 2.2(d) shows the detwinned martensite in free length after the detwinning load is removed. The free length difference between austenite and detwinned martensite is δ_M. The displacement δ_L is the length difference between loaded martensite and unloaded martensite under fully detwinned status.

In general, the NiTi spring actuation cycle starts in the martensite phase with an external load F. And then, the spring is activated by heating it up to transition temperature, which results in a spring length contraction under the load. The displacement created in this transformation is called effective displacement,$\delta_{\text{effective}}$ and calculated as follows:

$$\delta_{\text{effective}} = \delta_M + \delta_L - \delta_H \tag{1}$$

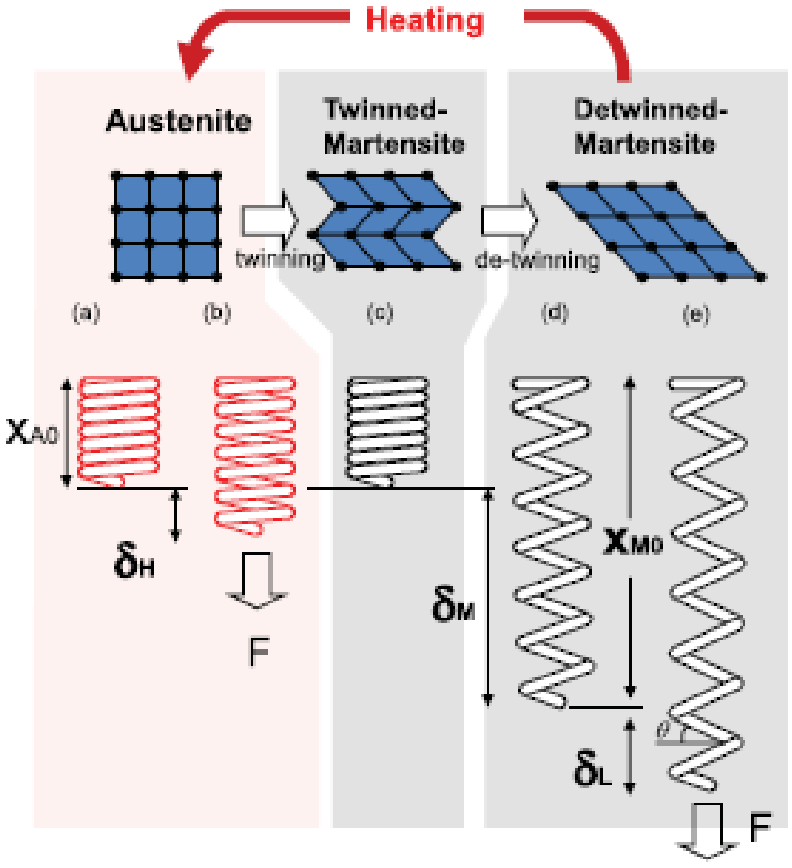

Fig. 2.2. Five representational states of a NiTi coil spring actuator: (a) full austenite without load (b) full austenite with load, (c) twinned martensite without load, (d) fully detwinned martensite without load, and (e) fully detwinned martensite with load.

Here, each δ_i value, where $i \in \{H, L, M\}$, corresponds to the displacement of the coil. Using the general coiled spring deflection equation, δ_i is a function of an external load F, overall spring diameter D, NiTi wire diameter d, number of active coils in the spring n, and the shear modulus of the spring after annealing G

$$\delta_i = \frac{8FD^3n}{Gd^4} \tag{2}$$

The shear strain γ of the spring is

$$\gamma = \frac{\tau}{G} \tag{3}$$

and the shear stress τ is

$$\tau = \frac{8FD\kappa}{\pi d^3} \tag{4}$$

where κ is a stress correction factor. From Wahl's formula [18],

$$\kappa = \frac{4C-1}{4C-4} + \frac{0.615}{C}. \tag{5}$$

Here C is the spring index, defined as follows:

$$C = \frac{D}{d}. \tag{6}$$

Using this analysis, the difference of the free length between the austenite and martensite phases δ_M can be calculated from (2) through (4) as

$$\delta_M = \frac{\pi\gamma D^2 n}{d\kappa}. \tag{7}$$

Therefore, for a given F, the effective displacement from (1) is given as follows:

$$\delta_{\text{effective}} = \frac{\pi\gamma D^2 n}{d\kappa} + \frac{8FD_{\text{eff}}^3 n}{G_M d^4} - \frac{8FD^3 n}{G_A d^4}. \tag{8}$$

There is a significant coil diameter D change when the coil spring is elongated under martensite phase with a load F. Therefore, to calculate the displacement properly in this situation, an effective spring diameter D_{eff} is used

$$D_{\text{eff}} = D\cos\theta$$

where θ is the angle between the spring wire and the horizontal plane.

2.1.3 Fabrication and Characterization of NiTi Coil Actuators

[16] The fabrication process of micro-NiTi coil muscle fibers is depicted schematically in Fig. 2.3. One end of a 200-μm diameter core wire and a 100-μm diameter NiTi wire [Dynalloy Flexinol (R)] are clamped at a drill press. Constant tension is applied to the core wire by attaching a weight on the free end. A metal tube and a bar attached to the tube make up the coil guide, which is essential for closely packing the NiTi coil on the core. The friction of the metal tube on the core acts against the tension from the coiled NiTi and keeps the core wire vertical.

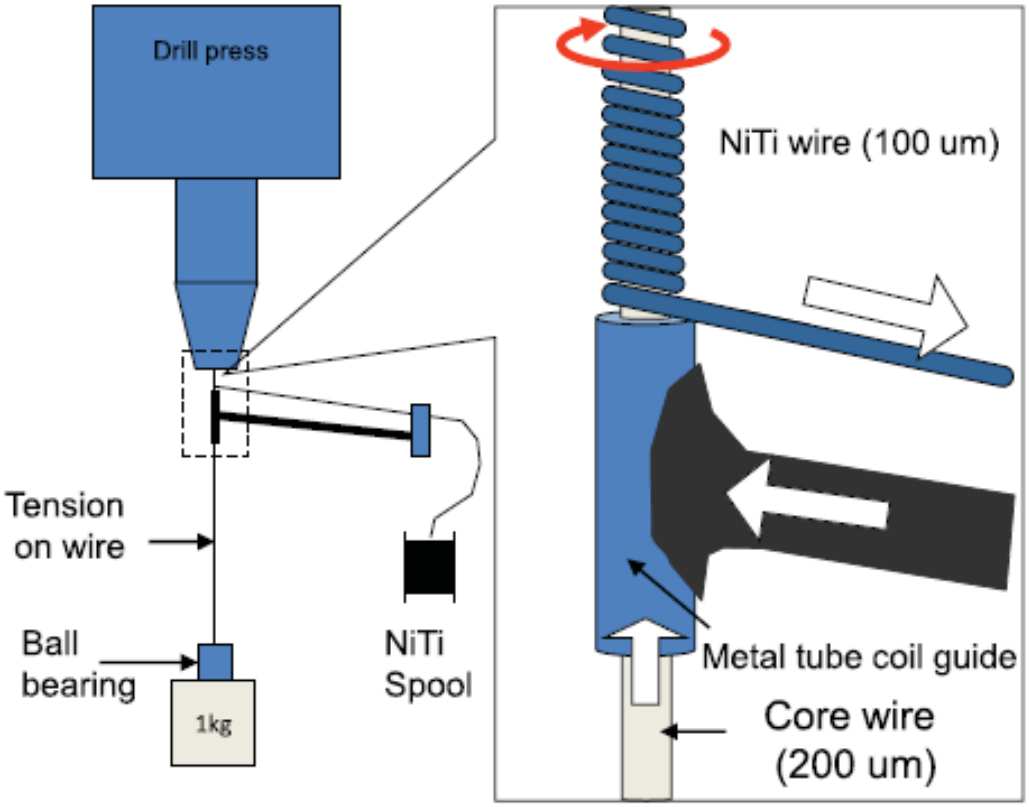

Fig. 2.3. Simple manufacturing system enables the fabrication of long strand coiled springs of NiTi muscle fiber. The core wire is under tension and a NiTi wire is wound around the core. The guidance tube is slightly larger than the core wire. The tension of the NiTi wire is maintained by friction between NiTi and the long bar.

After winding the NiTi wire to a given length, the ends of the coil are clamped to the core wire and annealed in an oven under a controlled temperature. The annealing temperature determines various parameters of the resulting spring actuator. Two noticeable trends are identified that vary with the annealing temperature: 1) increasing the annealing temperature decreases the detwinning force, and 2) large annealing temperatures cause the resulting springs to lose their ability to return to their original dimensions after loading.

Detwinning is a passive process that returns the actuated NiTi coils in the twinned martensite state back to the fully detwinned martensite state through martensite transformation. This requires external work, such that a certain amount of tensile force pulls the coils to extend them, transforming their state in the process. This force is strongly

dependant on the annealing temperature, and is a mechanical characteristic of the actuators. When used in an antagonistic configuration, such that the actuation of one coil detwins the other, this characteristic force requirement affects the full cycle work efficiency of the actuators.

We experimentally investigated the dependence of the detwinning force on the annealing temperature. 25-mm-long NiTi coil springs are annealed at nine different temperatures ranging from 300 ◦C to 540 ◦C in 30 ◦C increments. Weights are hanged on the coils to apply varying external forces. Weight application and removal were carried out slowly to reduce dynamic effects and the spring effect. The final elongated length was measured under no load, after the weights were removed.

Fig. 2.4(a) depicts the results. In these curves, detwinning is indicated as a plateau, similar to a plastic deformation behaviour in stress–strain curves. The value at which this plateau occurs is the detwinning force. This force clearly decreases with the increasing annealing temperature as a general trend. After detwinning, the coils yield a larger stiffness, indicated by a sharp gradient in the curve after the plateau. This stiffness change occurs at larger deflections as the annealing temperature is increased. We used an annealing period of 20 min for these experiments. We found no change in actuator characteristics above this value.

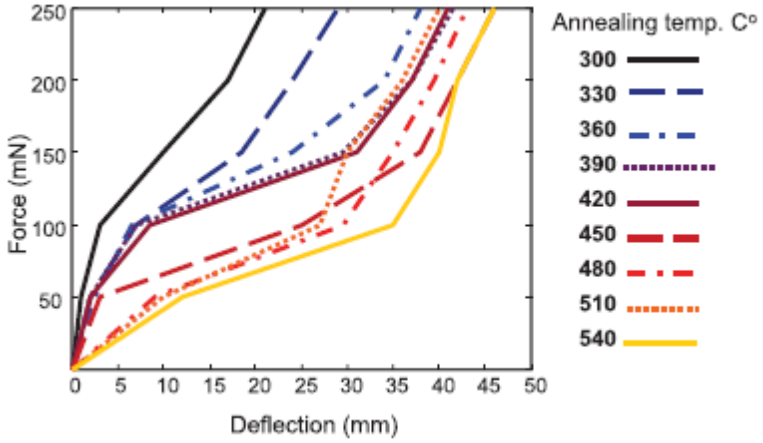

(a)

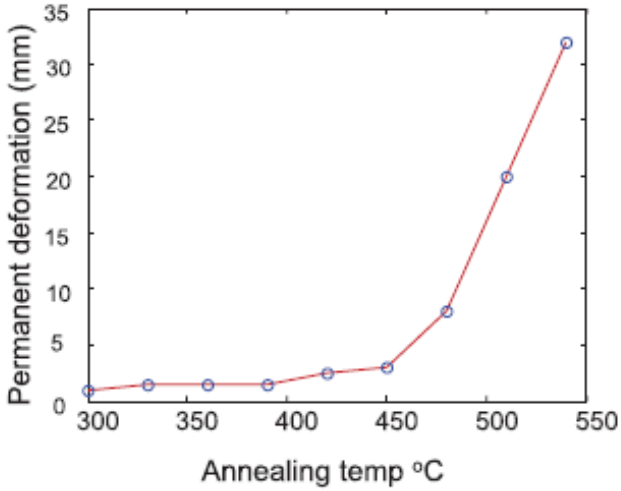

(b)

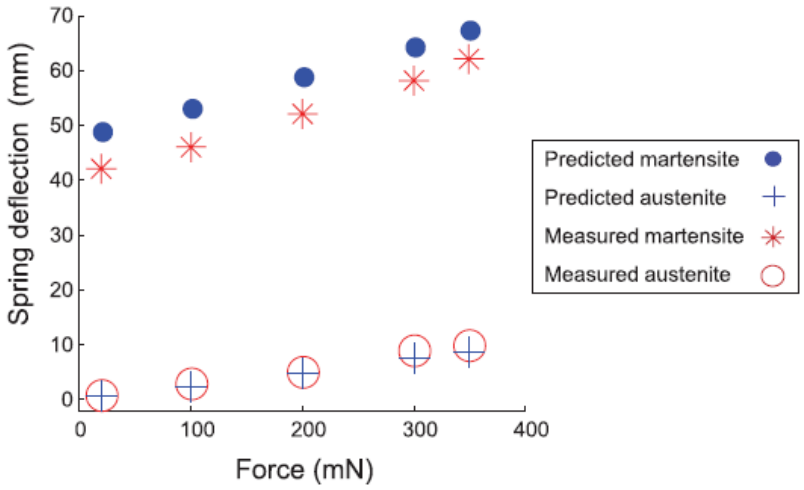

(c)

Fig. 2.4. Experimental results of NiTi coil spring. (a) Deflection of springs annealed at various temperatures under load. (b) Permanent plastic deformation of NiTi coil springs annealed at various temperatures, after lifting a 35-g weight. (c) Experimental NiTi coil spring deflection data are compared to the theoretical model predictions: Average errors in Martensite and Austenite phases' are−22% and 12.4%, respectively.

The second effect of the annealing temperature on the NiTi coil actuator operation is shown in Fig. 2.4(b). This is a curve of permanent deformation of these actuators, 25 mm in original length, after lifting a 35-g weight only once. The permanent deformation is measured as the difference between the final length in the austenite state after lifting and the original length of the coils. The data indicate that springs annealed at a temperature below 400 ◦C show reasonable consistency at multiple trials. In contrast, springs annealed at higher temperatures yield large permanent deformations after multiple trials. In short, even though higher annealing temperatures result in smaller detwinning forces, the original dimension is lost for springs annealed above 400 ◦C after a single lifting cycle, a trade off in fabrication. Based upon these observations, we used a NiTi coil spring annealed at 390 ◦C for further experiments. Weight lifting experiments are performed and stroke lengths are measured for comparison of the model output with experimental results. Fig. 2.4(c) displays our results of deflection of springs in both the austenite and the martensite states with various loads. We applied a constant current of 150 mA to maintain the spring in the austenite state under load. Model predictions from (2) are plotted with the experimental data. The shear modulus of NiTi is also a function of the annealing temperature. Thus, we calculated this value through the deflection length in the austenite state. As the martensite state shear modulus, we used a third of the austenite shear modulus, which is the typical case for NiTi [18].

The work done by the NiTi coil springs when they lift a known weight yields the energy density of these actuators. A 25 mm long NiTi coil annealed at 390 ◦C lifts a 37.9-g weight with a stroke length of 50 mm. The total energy to perform this task is then 0.0184 J. The weight of the NiTi coil is 0.014 g. Thus, the energy density, defined as the amount of work done by unit mass of this actuator in a single stroke, is calculated to be 1314 J/kg.

2.2 Requirement Analysis

The main and the foremost most import requirement for this project are the NiTi coils. Modelling of these springs are the most important as they serve as the actuators in the gripper. Initially, manufacturing of customised springs based on the equation (8), discussed in section 2.1.2, was proposed.

2.2.1 Initial Proposed Wire and Spring Specifications

The table below specifies the initial proposed wire (NiTi) specifications, used to manufacture the NiTi springs.

Diameter Size (Inches)	***Resistance (Ohms/ Inch)***	***Maximum Pull Force (grams)***	***Approximate Current at Room Temperature (mA)***	***Contraction Time (seconds)***	***Off Time LT=70°C Wire (seconds)***
0.004	8.0	150	180	1	0.8

The following wire specification was selected due to its low resistance, low contraction time and low off time. Lower the contraction time and off time, faster would be the actuation of the springs.

Initially customised springs were proposed which were of different lengths. This was because the NiTi coils were to be attached between the joints of the fingers. But, since the length between the joints of a human finger is different hence four springs of different solid lengths for a single finger was proposed. Since we required an approximate displacement of 5mm by the NiTi coils during its actuation, hence the length of the coil in various phases (martensite and austenite) were calculated according to the equation (8) given in section 2.1.2.

The table below gives the specification of NiTi coils for the back side and palm side of the hand.

Back Side		
	Spring 1	Spring 2
Spring Diameter	285µm	285µm
Solid Length	20mm	17.5mm
End Conditions	Hooks	Hooks
Cold-Loaded Length	26.7116 mm	24.2119 mm
Hot Loaded Length	21.812 mm	19.312 mm
Clearance	0.158202 mm	0.0009179 mm
Number of Turns	167.76	167.76

Palm Side		
	Spring 1	Spring 2
Spring Diameter	350µm	350µm
Solid Length	15mm	10mm
End Conditions	Hooks	Hooks
Cold-Loaded Length	21.712 mm	16.712 mm
Hot Loaded Length	16.812 mm	11.812 mm
Clearance	0.05787 mm	0.0026716 mm
Number of Turns	90.58	90.58

2.2.1.1 Cost Associated

DYNALLOY, Inc. (a company dedicated to providing products related to Dynamic Alloys) offered to help us and provide customise springs made up of NiTi, sold with the name of Flexinol. We required about 5-6 each type of springs, so we require around 20 springs altogether. A technical associate at the company studied our specifications and estimated the overall cost of production of customised NiTi coils to be around $10000. This was a high cost to be accustomed to as we wanted our product to be cheap and affordable. Hence we shifted to the use of standard springs which was provided by the company. This helped us in decreasing the overall cost of the springs by almost 80 percent. But in order to make use of standard Flexinol springs, we needed some changes in our design.

2.2.2 Designing of the Coil Actuators using Standard NiTi Springs

[19] DYNALLOY, Inc. provides NiTi products under the trade name of Flexinol®. Flexinol® Actuator Wires are small diameter wires which contract like muscles when electrically driven. Smaller than motors or solenoids, cheaper and generally easier to use, these wires perform physical movement across an extremely wide variety of applications.

Flexinol® is a trade name for shape memory alloy actuator wires. Made of nickel-titanium these small diameter wires contract like muscles when electrically driven. This ability to flex or shorten is characteristic of certain alloys that dynamically change their internal structure at certain temperatures. The idea of reaching higher temperatures electrically came with the light bulb, but instead of producing light these alloys contract by several percent of their length when heated and can then be easily stretched out again as they cool back to room temperature. Like a light bulb both heating and cooling can occur quite quickly. The contraction of Flexinol® actuator wires when heated is opposite to ordinary thermal expansion, is larger by a hundredfold, and exerts tremendous force for its small size. The main point is that movement occurs through an internal "solid state" restructuring in the material that is silent, smooth, and powerful.

2.2.2.1 Stretch Ratio

Flexinol® actuator springs can be an alternative to straight Flexinol® actuator wires for applications with low force and high travel requirements. These springs can

contract and relax multiples of their length. When Flexinol® actuator springs are used within the correct range then obtaining repeatable motion from the springs for millions of cycles is reasonable.

[19] Stretch Ratio “SR” is defined as any length “L" over the solid length “SL", in any state, hot or cold. For example a spring with a SR of 4 cold and 2 hot, assuming a solid length “SL” of 10mm would then be 20mm hot, and 40mm cold.

$$SR = L/SL$$

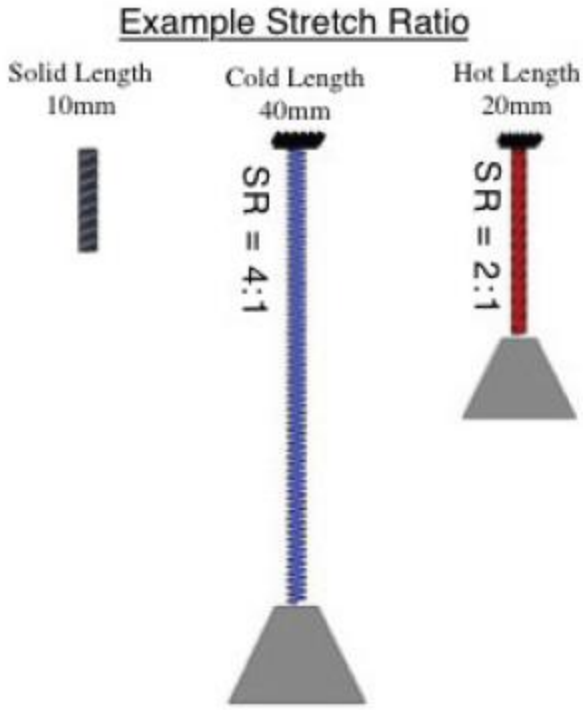

Fig. 2.5. Represents an example of Stretch Ratio.

2.2.2.2 New Spring Specifications

The following are the specifications of the Flexinol® springs used in the robotic gripper. The specifications also give us a rough idea as to how much current and force to expect with spring of given diameter. The data has been taken from the technical datasheet provided by Dynalloy, Inc.

Spring Wire Diameter: 0.203mm

Outer Diameter: 1.37mm

SR Cold, SR Hot: 14, 5

Displacement/ Coil: 1.8mm

Resistance on Straight Wire: 29.13ohms/meter

*Heating Pull Force: 39.3grams

*Cooling Deformation Force: 15.94grams

Approximate Current for 2 Seconds Contraction: 0.7A

**Cooling Time 90°C “HT” Wire: 3.0 sec

We can calculate the number of turns of the spring using the following formula:

$$Number\ of\ coils * Wire\ diameter = Solid\ Length$$

Dynalloy, Inc. provides standard springs with three different wire diameters. The springs with the above described wire diameter (0.203mm) is best suited, as it fulfils the pull force required by the gripper to perform the grasp and release action. Secondly, the spring has the minimum cooling time of the three available springs.

*The Heating pull force is based on ~ 25,000 psi, which for many applications is maximum safe stress for the wire. The cooling deformation force is based on ~ 10,000 psi, which is a good starting point in the design.

The contraction time is directly related to current input. The figures used here are only approximate since room temperatures, air current and heat sinking of specific devices vary.

*Approximate cooling time is at room in static air, using a vertical spring. The last 0.5% of deformation is not used in these approximations. “HT” = High Temperature Flexinol® Actuator Spring.

2.3 Feasibility Analysis

2.3.1 Operational Feasibility

The movement or stroke of Flexinol® actuator wire is measured as a percentage of the length of the wire being used and is determined, in part, by the level of stress one uses to reset the wire, or to stretch it in its low temperature phase. This opposing force, used to stretch the wire, is called the bias force. In most applications, the bias force is exerted on the wire constantly, and on each cycle as the wire cools, this force elongates it. If no force is exerted as the wire cools, very little deformation or stretch occurs in the cool, room temperature state and correspondingly very little contraction occurs upon heating. Up to a point the higher the load the higher the stroke. The strength of the wire, its pulling force and the bias force needed to stretch the wire back out are a function of the wire size or cross sectional area and can be measured in pounds per square inch or “psi”. [19] If a load of 5,000 psi (34.5 MPa) is maintained during cooling, then about 3% memory strain will be obtained. At 10,000 psi (69 MPa), about 4% results, and with 15,000 psi (103 MPa) and above, nearly 5% is obtained. However, there is a limit to how much stress can be applied.

Far more important to stroke is how the wire is physically attached and made to operate. Dynamics in applied stress and leverage also vary how much the actuator wires move. While normal bias springs that increase their force as the Flexinol® actuators contract have only 3-4% stroke, reverse bias forces which decrease as the actuator wires contract can readily allow the wire to flex up to 7%. Mechanics of the device in which it is used can convert this small stroke into movements over 100% of the wires' length and

at the same time provide a reverse bias force. The stress or force exerted by Flexinol® actuator wires is sufficient to be leveraged into significant movement and still be quite strong. Some basic structures and their percent of movement, are as follows:

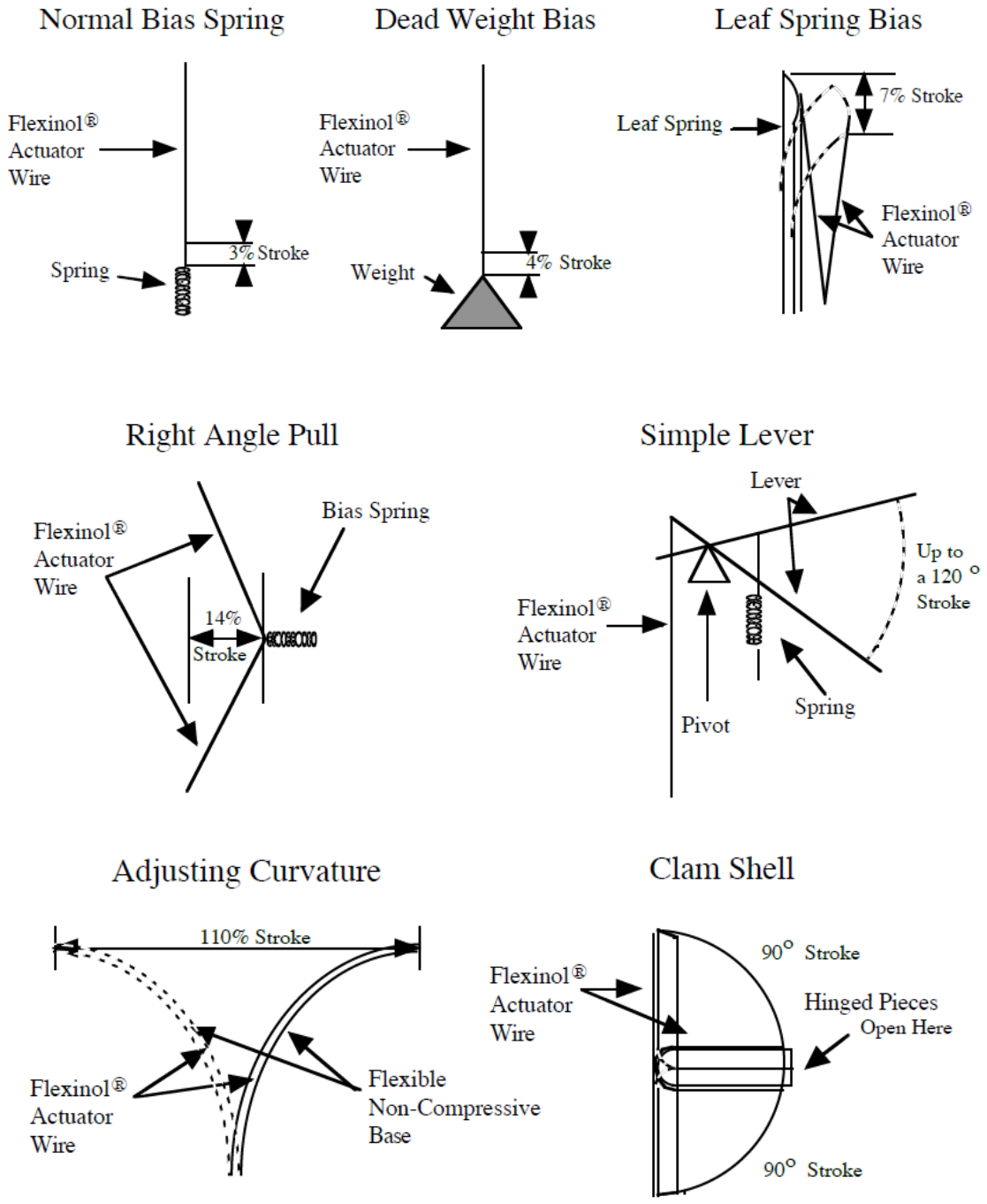

Fig. 2.6. Representation of various basic structures and the percentage of movement of NiTi wire/coils.

2.3.2 Electrical Guidelines

[19] If Flexinol® actuator wire is used in the appropriate conditions, then obtaining repeatable motion from the wire for tens of millions of cycles is reasonable. If higher stresses or strains are imposed, then the memory strain is likely to slowly decrease and good motion may be obtained for only hundreds or a few thousands of cycles. The permanent deformation that occurs in the wire during cycling is heavily a function of the stress imposed and the temperature under which the actuator wire is operating. Flexinol® wire has been specially processed to minimize this straining, but if the stress is too great or the temperature too high, some permanent strain will occur. Since temperature is directly related to current density passing through the wire, care should be taken to heat, but not overheat, the actuator wire. The following charts give rough guidelines as to how much current and force to expect with the wire, with diameter of 0.203mm (as stated in section 2.2.2.2) used in the manufacturing of our springs.

Diameter Size (mm)	***Resistance (Ohms/ meter)***	***Pull Force (grams)***	***Cooling Deformation Force* (grams)***	***Approximate** Current for 1 Second Contraction (mA)***	***Cooling Time 194°F, 90°C "HT" Wire (seconds)***
0.203	29	570	228	660	1

* The Heating pull force is based on 25,000 psi (172 MPa), which for many applications is the maximum safe stress for the wire. However, many applications use higher and lower stress levels. This depends on the specific conditions of a given design. The cooling deformation force is based on 10,000 psi (70 MPa), which is a good starting point in a design. Nonetheless, this value can also vary depending on how the material is used.
** The contraction time is directly related to current input. The figures used here are only approximate since room temperatures, air currents, and heat sinking of specific devices vary. On small diameter wires (<= 0.006" diameter) currents that heat the wire in 1 second can typically be left on without over-heating it.
*** Approximate cooling time, at room temperature in static air, using a vertical wire. The last 0.5% of deformation is not used in these approximations.

2.3.3 Cycle Time

The contraction of the Flexinol® actuator wire is due solely to heating and the relaxation solely to cooling. Both contraction and relaxation are virtually instantaneous with the temperature of the wire. As a result mechanical cycle speed is dependent on and directly related to temperature changes. Applying high currents for short periods of time can quickly heat the wire. It can be heated so fast in fact that the limiting factor is not the rate at which heating can occur but rather the stress created by such rapid movement. If the wire is made to contract too fast with a load, the inertia of the load can cause over stress to the wire. To perform high speed contractions inertia must be held low and the current applied in short high bursts. Naturally, current which will heat the wire from room

temperature to over 212 °F (100°C) in 1 millisecond, will also heat it much hotter if left on for any length of time [19].

While each device has quite different heat sinking and heating requirements, a simple rule of thumb test can be used to prevent overheating. Measuring the actual internal temperature of the wire across such short time periods is somewhat problematic, however, one can tell if the actuator wire is overheated simply by observing if the wire immediately begins to cool and relax when the current is shut off or not.

If it does not begin to relax and elongate under a small load promptly, when the power is cut, then the wire has been needlessly overheated and could easily be damaged. Simple visual observation is all that is needed to design measured heating circuitry.

Flexinol® actuator wire has a high resistance compared to copper and other conductive materials but is still conductive enough to carry current easily. In fact one can immerse the wire in regular tap water and enough current will readily flow through it to heat it. All of the conventional rules for electrical heating apply to the wire, except that its resistance goes down as it is heated through its transformation temperature and contracts. This is contrary to the general rule of increased resistance with increased temperature. Part of this drop in resistance is due to the shortened wire, and part is due to the fact that the wire gets thicker as it shortens, roughly maintaining its same three-dimensional volume. It makes no difference to the wire whether alternating current, direct current, or pulse width modulated current is used.

Again relaxation time is the same as cooling time. Cooling is greatly affected by heat sinking and design features. The simplest way to improve the speed of cooling is to use smaller diameter wire. The smaller the diameter the more surface to mass the wire has and the faster it can cool. Additional wire, even multiple strands in parallel, can be used in order to exert whatever force is needed. The next factor in improving the relaxation or cooling time is to use higher temperature wire. This wire contracts and relaxes at higher temperatures. Accordingly the temperature differential between ambient or room temperature and the wire temperature is greater and correspondingly the wire will drop below the transition temperature faster in response to the faster rate of heat loss.

Other methods of improved cooling are to use: forced air, heat sinks, increased stress (this raises the transition temperature and effectively makes the alloy into a higher transition temperature wire), and liquid coolants. Combinations of these methods are also effective. Relaxation time can range from several minutes (i.e. delay switches) to fractions of milliseconds (i.e. miniature high speed pumps) by effective and proper heat sinking.

Better cooling methods are likely to require more current or heat to move and/or hold the wire in an "on" position. In some cases one may wish to quickly turn the wire on (that is electrically heat it until it contracts) then hold it on for some time. This will likely require a two-step driving current with a larger current to heat the wire and a reduced current to keep it hot without overheating it. There are a number of simple circuits, which will do this.

Chapter 3.
SYSTEM ANALYSIS, MODELLING AND DESIGN

3.1 System Analysis

The robotic gripper is inspired by the structure and movement of the human hand. Hence in order to model a gripper based on the anatomy of the hand, a basic study of the structure of the hand that aid in its movement is necessary.[20] The muscles in the forearm and palm (thenar muscles) all work together to keep the wrist and hand moving, stable, and aligned. The image below shows the bones from the back side of the hand. The red lines show where the tendons attach the muscles to the bones.

The muscles that move the fingers and thumb are above the wrist in the forearm. Long flexor tendons extend from the forearm muscles through the wrist and attach to the small bones of the fingers and thumb. When you bend or straighten your finger, these flexor tendon slide through a snug tunnel, called the tendon sheath that keeps the tendon in place next to the bones.

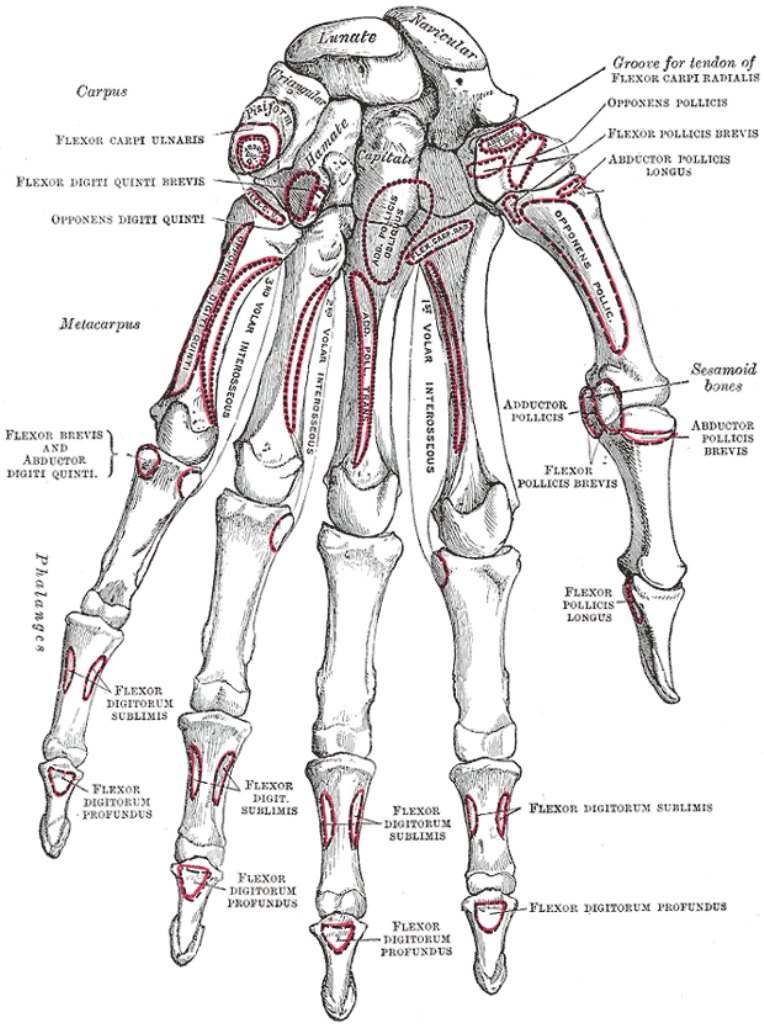

Fig. 3.1. Bones of the left hand (Volar Surface)

Tendons are white, flexible fibrous cords at the ends of muscles that attach the muscles to the radius, ulna, carpals, metacarpals and phalanges. When the muscles

contract, they pull on the tendons to move the bone. The tendons that run down our fingers are held in place by a series of ligaments, called pulleys that arch over the tendons forming a “tunnel-like” sheath. Normally, the tendons glide easily through the tunnel. Some tendons also serve as stabilizers.

A series of ligaments in a tunnel-like arrangement hold the tendons in place on the bones. A slippery coating, called tenosynovium, surrounds the tendons and keeps the tendons moving smoothly under the ligaments when the hand grasps objects.

3.2 Modelling of the Spring Actuator

Here the NiTi coils are used to perform the functionality of the muscles and tendons. Two sets of springs of different turns are used. One set of springs represent the tendons on the forearm and the other represent the tendons on the palm side of the hand. Two different sets of springs of different turns are required because the springs counteract each other to produce the grasp and release action.

The solid length (“SL”) of the spring is decided according to the length of the spring in its austenite phase. When the gripper performs the grasp action the springs attached on the palm surface gets actuated to its austenite phase. According to the finger model described in section 3.3, then length of the spring in its various phases using the specifications defined in section 2.2.2 of Chapter 2 are as follows:

SR Cold, SR Hot: 14, 5

Length in austenite phase: 10mm

Solid Length: 2mm

Length in martensite phase: 28mm

Number of turns: 10

Similarly, when the gripper performs the release action, the springs on the forearm get actuated to its austenite phase. Hence the length for the second set of springs in their various phases based on the specifications described in section 2.2.2.2 and are given as follows:

SR Cold, SR Hot: 14, 5

Length in austenite phase: 22mm

Solid Length: 4.4mm

Length in martensite phase: 61.6mm

Number of turns: 21.67

3.3 Modelling of the Fingers of the Gripper

Inspired by the skeletal structure of the human hand, we present an antagonistic actuation mechanism which utilises the NiTi coils as muscle fibers and tendons as discussed in the previous section. This approach is used in the modelling, fabrication and development of a three finger gripper that behaves similar to human hand.

The three finger are designed to represent the index finger, middle finger and the thumb of a human hand. The gripper produces a grasp and release action similar to a human hand on the passage of an electrical impulse. When an electrical impulse is passed, one set of the NiTi coil actuators contracts while the other set is relaxed. Depending upon which set of the actuators gets contracted the gripper performs the grasp or release action.

3.3.1 Designing of the Finger Link

The human hand has a complex structure made up of 27 individual bones: 8 carpal bones, 5 metacarpal bones and 14 finger bones (also called phalanges) are connected by joints and ligaments. [22] The hand can be viewed in three sections by joint function:

- Carpus and wrist
- Metacarpus
- Fingers or phalanges

The links in the robotic gripper represent the phalanges and the metacarpus of a human hand. But, unlike the human hand in which the phalanges and the metacarpus are of different sizes, the links used in the robotic gripper are of same shape and size. This has been done to reduce complexity and introduce symmetry in the model. The link is modelled using SolidWorks. Fig. 3.2 shows a model of the link with all its dimensions.

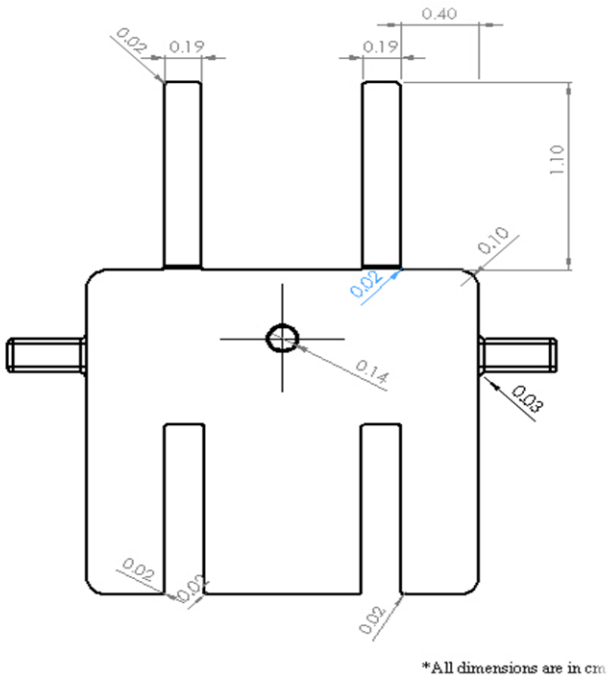

(a)

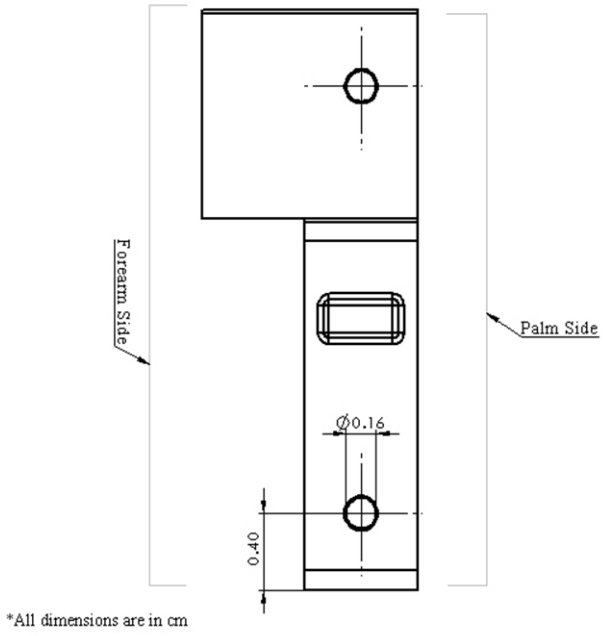

(b)

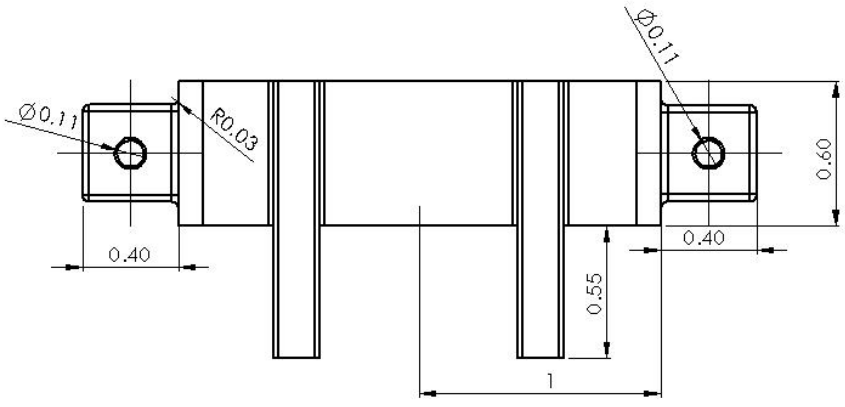

(c)

Fig. 3.2. The following figure represent the three views of the finger link (a) Front view. (b) Left view. (c) Top view.

3.3.2 Fabrication of the Links

The fabrication of the link includes the development of the link through a 3D printer. We used $Ultimaker^2$ for the purpose of 3D printing. $Ultimaker^2$ is the successor of $Ultimaker\ Orignal$ [as seen in Fig. 3.3 (a)]which works on fused filament fabrication (FFF) printing technology. It uses a software *Cura*, which is the 3D model to toolpath Slicer. The printing filament used to create the 3D model for this project is PLA (Ploylactic acid) [Fig. 3.3 (b) shows a spool of PLA filament]. [23] PLA is a bio-degradable polymer that can be produced from lactic acid, which can be fermented from crops such as maize. PLA is harder than ABS, melts at a lower temperature (around 180°C to 220°C) and has a glass transition temperature between 60-65°C. It does have a slightly higher coefficient of friction in the drive and transport than ABS, but this is more compensated for by its lower viscosity when molten.

(a)

(b)

Fig. 3.3. (a) Ultimaker2 used for 3D printing (b) Spools of PLA, used as the printing filament.

The NiTi springs during a phase transformation from martensite to austenite on actuation reach a temperature of around 70°C. At such a high temperature the model could rupture and break as PLA reaches its glass transition temperature. Thus to avoid this, the whole model is wrapped around with a high temperature tape. We used Kapton tape which is made from Kapton® polyimide film with silicon adhesive. They are compatible with a wide range of temperatures as low as -269°C and as high as 260°C. Thus they act as thermal insulators and protect the model from the NiTi coils during its actuation.

3.3.3 Construction of the Finger of the Gripper

The human hand consist of phalanges (fingers) and metacarpus. Each finger has three individual bones of different lengths. Construction of the fingers of the gripper in the similar fashion is a tough challenge, since links of different lengths would require springs of different number of coils. This increases the cost of the springs to a great extent. Hence a sustainable solution to the problem has been proposed. Unlike the bones of the human hand, all the links of the gripper will be of same shape and length. This helped in reducing the cost of the springs by a factor of approximately 80.

The finger of the gripper consists of four links. Three representing the phalanges and one the metacarpus. Fig. 3.5 shows a fully constructed finger of the gripper. The links are connected to each other by attaching the extrusion, marked as (a) in the Fig. 3.4, of one link to the section marked as (b) of the other link. When the Hole 1 [See Fig. 3.4] of one link is aligned in parallel with the Hole 2 of the other link, a wire is passed through these holes to provide movement to the link. Finally, the links are joined together through screws.

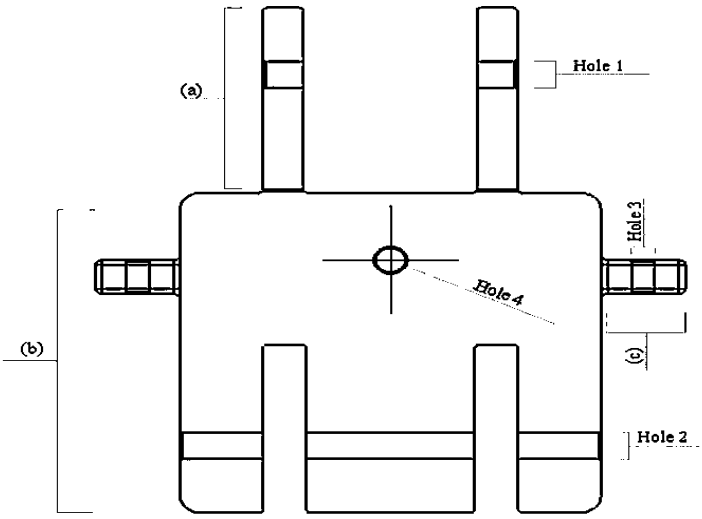

Fig. 3.4. Representation of the various components in the link model.

As discussed earlier in section 3.3, we require two sets of springs of different number of coils. The NiTi coils of solid length 4.4mm, are attached to the forearm side [See Fig. 3.2 (b)] of the link while the coils of solid length 2mm are connected to palm side of the link. The NiTi coils are attached between two links. One end of the NiTi muscle coil is fixed in Hole 4 [See Fig. 3.4] of one link and the other end is fixed in the Hole 4 of the other link.

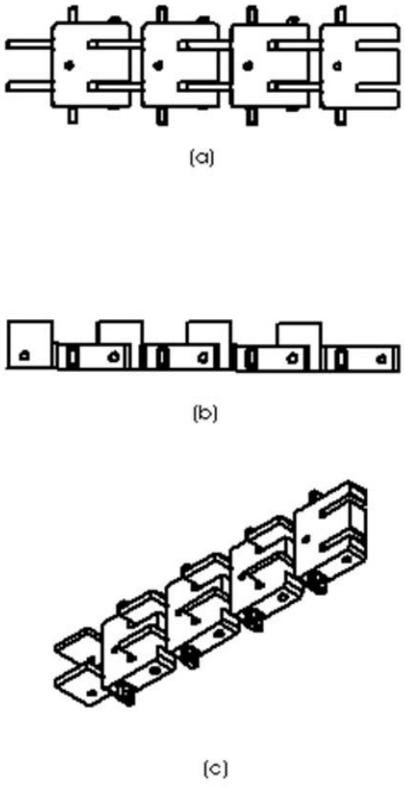

Fig. 3.5. Assembly of links to form a finger (a) Front view. (b) Left View. (c) Isometric View

The Fig. 3.5 represents an assembly of links joined together to form a finger of the gripper. As we can see in Fig. 3.5 (b), representing the left view of the finger, the extrusion on the forearm side of part (a) [as shown in Fig. 3.5], would help the finger to return and stay in a straight alignment during release action. Further, the last link to the finger is permanently fixed to the base of the gripper (discussed in next section).

3.3.4 Designing and Modelling of the Gripper Base

In biology, dactyly is the arrangement of digits (fingers and toes) on the hands, feet, or sometimes wings of a tetrapod animal. It comes from the Greek word δακτυλος = "finger". Sometimes the ending "-dactylia" is used. The derived adjectives end with "-dactyl" or "-dactylous". Anisodactyl is the most common arrangement of digits in birds, with three toes forward and one back. This is common in songbirds and other perching birds, as well as hunting birds like eagles, hawks, and falcons.

The arrangement of fingers in the robotic gripper is inspired by those of anisodactyl. The only difference is that instead of having three forward fingers, our gripper has only two forward fingers and one finger at the back. Three fingers are symmetrically placed such that the back finger is in between the two forward fingers [See Fig. 3.6 (a)]. The model of the base of the gripper (as shown in Fig. 3.6) was developed using SolidWorks.

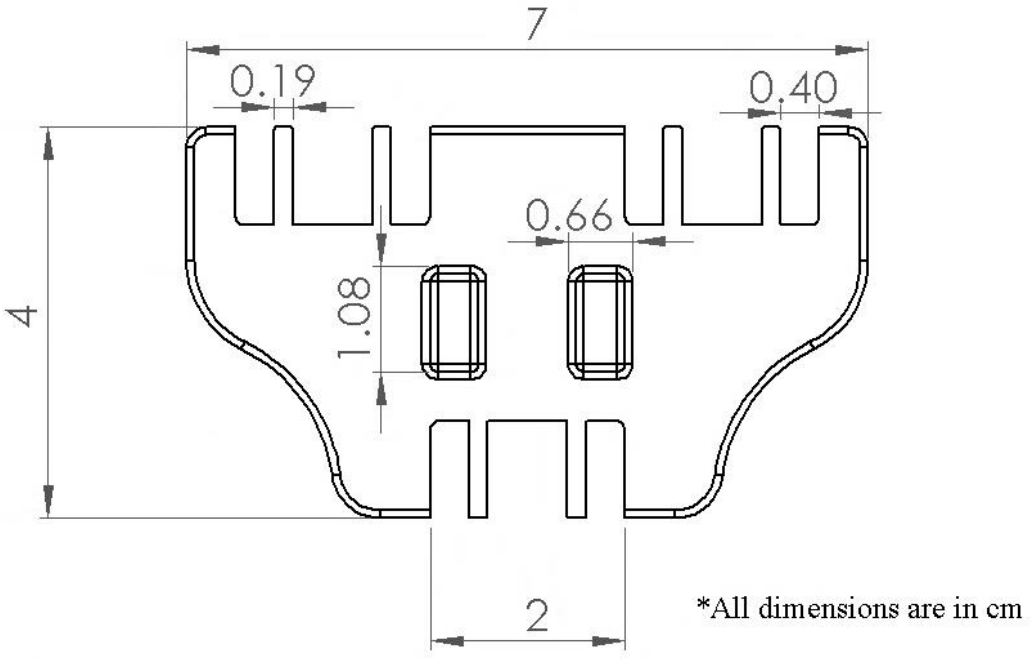

(a)

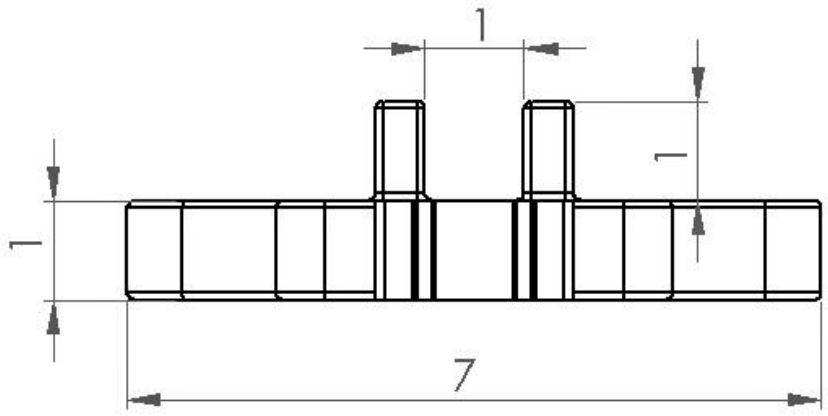

*All dimensions are in cm

(b)

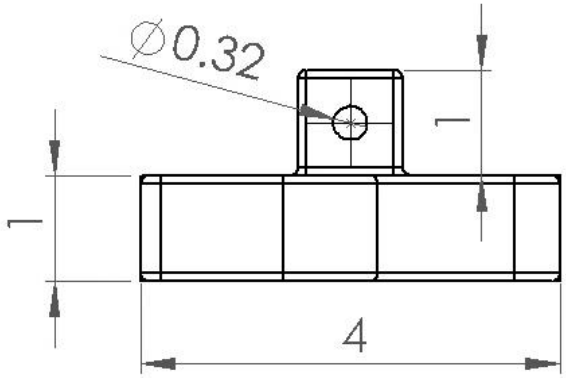

*All dimensions are in cm

(c)

Fig. 3.6. Model of the base of the gripper. (a) Top View. (b) Front View. (c) Left View.

The extrusion seen in Fig. 3.6 (b), of 1 cm length and 0.50 cm thickness, has been provided so that an external arm can be connected to the gripper. The hole in Fig. 3.6 (c) is used to connect the T joint of the arm to the base of the gripper using a M3 type screw. Hence the robotic gripper can be either used independently or combined with a robotic arm for complex operations. The base of the gripper is 3D printed using $Ultimaker^2$ using PLA as the printing filament.

3.4 Assembling of the Three Finger Gripper

The Fig. 3.7(a) shows the fully connected fingers of the gripper. The NiTi coil actuators are jointed on both sides of each finger using screws. The finger links are wrapped in Kapton tape to prevent any direct contact of the spring with the links. The links are connected to each other using a wire and screws, which not only holds the links together but also provides easy movement of the links in the vertical direction.

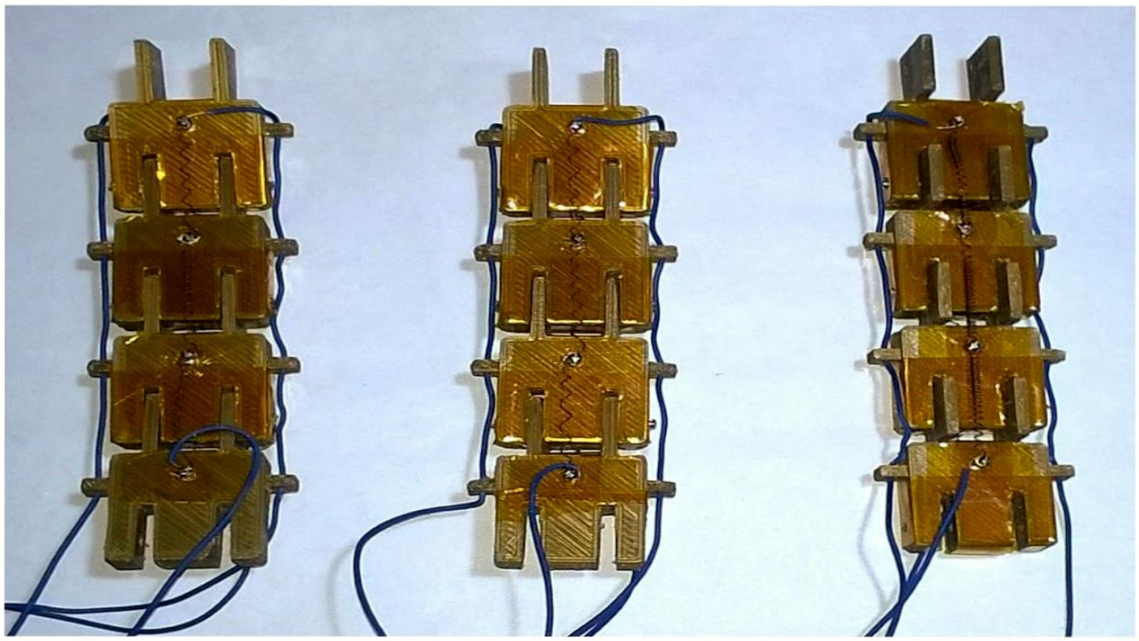

(a)

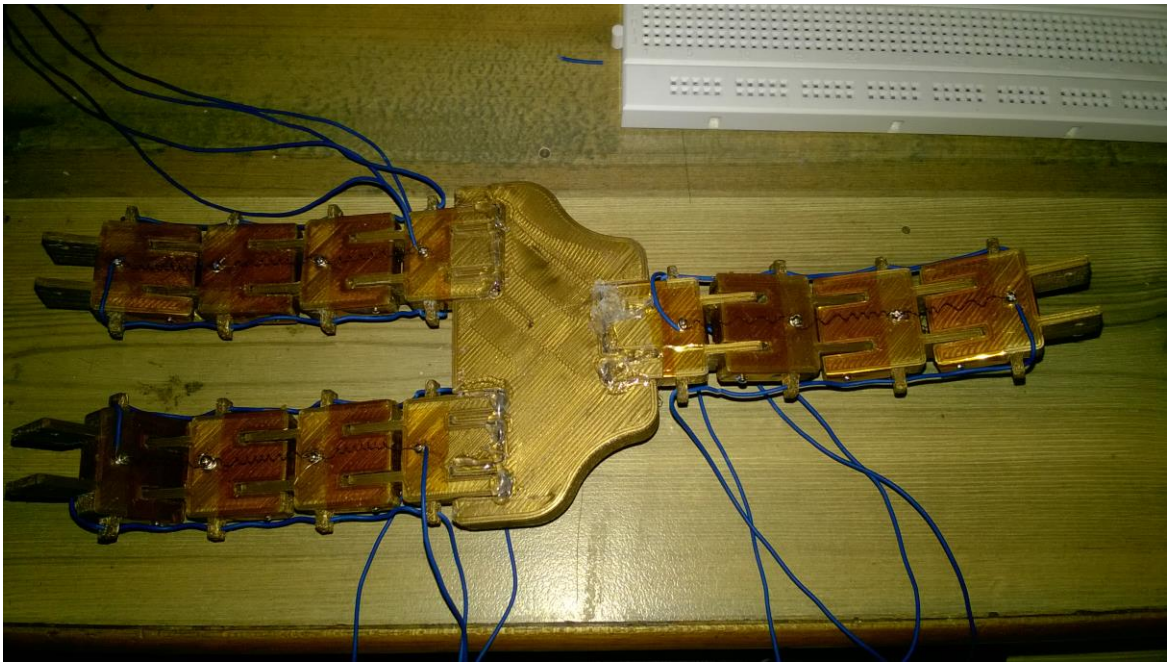

(b)

Fig. 3.7. (a) Shows the three fingers of the gripper. (b) Completely assembled gripper.

The last link of every finger is permanently fixed to the base of the gripper using a hot glue gun. The Fig. 3.7 (b) shows a completely assembled robotic gripper. Wires are also connected to the fingers of the gripper to provide an electrical connection, later discussed in the report.

Chapter 4.
HARDWARE AND SOFTWARE SPECIFICATIONS

4.1 Hardware Specifications

The NiTi coils require constant current of 0.7A for two seconds, as stated in section 2.2.2.2, for actuation. Hence the gripper requires a circuit that can control the current for two seconds and then turn the supply off on demand in order to achieve the grasp and release motion. The following are the components required for construction of such a circuit:

- Tiva™ TM4C123GH6PM Microcontroller from Texas Instruments.
- BC368 NPN Transistors.
- LM2596 DC-DC Buck Converter Step-Down Power Module.
- Resistors of 1Ω and 2Ω resistances.
- 11.1V 5Ah (55.5Wh) Li-Ion Battery.
- Breadboard.
- Jumper wires.

4.1.1 BC368 NPN General Purpose Amplifier

[25] This device is designed for general purpose medium power amplifiers and switches requiring collector currents to 1.5 A. Fig. 4.1 shows the BC368 NPN transistor with its configuration. Below are the ratings and characteristics associated with BC368.

*Absolute Maximum Ratings**

TA = 25°C unless otherwise noted

Symbol	Parameter	Value	Units
V_{CEO}	Collector-Emitter Voltage	20	V
V_{CES}	Collector-Base Voltage	25	V
V_{EBO}	Emitter-Base Voltage	5.0	V
I_C	Collector Current - Continuous	2.0	A
T_J, T_{stg}	Operating and Storage Junction Temperature Range	-55 to +150	°C

*These ratings are limiting values above which the serviceability of any semiconductor device may be impaired.

NOTES:

1. These ratings are based on a maximum junction temperature of 150 degrees C.
2. These are steady state limits. The factory should be consulted on applications involving pulsed or low duty cycle operations.

Thermal Characteristics

TA = 25°C unless otherwise noted

Symbol	Characteristic	Max	Units
		BC368	
P_D	Total Device Dissipation Derate above 25°C	625 5.0	mW mW/°C
$R_{\theta JC}$	Thermal Resistance, Junction to Case	83.3	°C/W
$R_{\theta JA}$	Thermal Resistance, Junction to Ambient	200	°C/W

Fig. 4.1. BC368 NPN General Purpose Amplifier with its Base, Collector and Emitter marked as B, C and E respectively.

Electrical Characteristics

TA = 25°C unless otherwise noted

Symbol	Parameter	Test Condition	Min	Max	Units
OFF CHARATERISTICS					
$V_{(BR)CEO}$	Collector-Emitter Breakdown Voltage	I_C = 10mA, I_B = 0	20		V
$V_{(BR)CES}$	Collector-Base Breakdown Voltage	I_C = 10µA, I_E = 0	25		V
$V_{(BR)EBO}$	Emitter-Base Breakdown Voltage	I_E = 10µA, I_C = 0	5.0		V
I_{CBO}	Collector-Cutoff Current	V_{CB} = 25V, I_E = 0 V_{CB} = 25V, I_E = 0, T_A = 150°C		10 1.0	µA mA
I_{EBO}	Emitter-Cutoff Current	V_{EB} = 5.0V, I_C = 0		10	µA
ON CHARATERISTICS					
h_{FE}	DC Current Gain	I_C = 5.0mA, V_{CE} = 10V I_C = 0.5A, V_{CE} = 1.0V I_C = 1.0A, V_{CE} = 1.0V	50 85 60	 375 	
$V_{CE(sat)}$	Collector-Emitter Saturation Voltage	I_C = 1.0A, I_B = 100mA		0.5	V
$V_{BE(on)}$	Base-Emitter On Voltage	I_C = 1.0A, V_{CE} = 1.0V		1.0	V
SMALL SIGGNAL CHARATERISTICS					
f_T	Current Gain-Bandwidth Product	I_C = 10mA, V_{CE} = 5.0V, f=35MHz			

4.1.2 Tiva™ TM4C123GH6PM Microcontroller

[25] Texas Instrument's Tiva™ C Series microcontrollers provide designers a high-performance ARM® Cortex™-M-based architecture with a broad set of integration capabilities and a strong ecosystem of software and development tools. Targeting performance and flexibility, the Tiva™ C Series architecture offers an 80 MHz Cortex-M with FPU, a variety of integrated memories and multiple programmable GPIO. Tiva™ C Series devices offer consumers compelling cost-effective solutions by integrating application-specific peripherals and providing a comprehensive library of software tools which minimize board costs and design-cycle time.
The Tiva™ C Series ARM Cortex-M4 microcontrollers provide top performance and advanced integration. The product family is positioned for cost-conscious applications requiring significant control processing and connectivity capabilities such as:

- Low power, hand-held smart devices
- Gaming equipment
- Home and commercial site monitoring and control
- Motion control
- Medical instrumentation
- Test and measurement equipment
- Factory automation
- Fire and security
- Smart Energy/Smart Grid solutions
- Intelligent lighting control
- Transportation

For applications requiring extreme conservation of power, the TM4C123GH6PM microcontroller features a battery-backed Hibernation module to efficiently power down the TM4C123GH6PM to a low-power state during extended periods of inactivity. With a power-up/power-down sequencer, a continuous time counter (RTC), multiple wake-from-hibernate options, a high-speed interface to the system bus, and dedicated battery-backed memory, the Hibernation module positions the TM4C123GH6PM microcontroller perfectly for battery applications.

In addition, the TM4C123GH6PM microcontroller offers the advantages of ARM's widely available development tools, System-on-Chip (SoC) infrastructure IP applications, and a large user community. Additionally, the microcontroller uses ARM's Thumb®-compatible Thumb-2 instruction set to reduce memory requirements and, thereby, cost. Finally, the TM4C123GH6PM microcontroller is code-compatible to all members of the extensive Tiva™ C Series; providing flexibility to fit precise needs.

4.1.2.1 TM4C123GH6PM Microcontroller Overview

The TM4C123GH6PM microcontroller combines complex integration and high performance with the features shown in figure below [25].

Feature	Description
Core	ARM Cortex-M4F processor core
Performance	80-MHz operation; 100 DMIPS performance
Flash	256 KB single-cycle Flash memory
System SRAM	32 KB single-cycle SRAM
EEPROM	2KB of EEPROM
Internal ROM	Internal ROM loaded with TivaWare™ for C Series software
Communication Interfaces	
Universal Asynchronous Receivers/Transmitter (UART)	Eight UARTs
Synchronous Serial Interface (SSI)	Four SSI modules
Inter-Integrated Circuit (I^2C)	Four I^2C modules with four transmission speeds including high-speed mode
Controller Area Network (CAN)	Two CAN 2.0 A/B controllers
Universal Serial Bus (USB)	USB 2.0 OTG/Host/Device
System Integration	
Micro Direct Memory Access (µDMA)	ARM® PrimeCell® 32-channel configurable µDMA controller
General-Purpose Timer (GPTM)	Six 16/32-bit GPTM blocks and six 32/64-bit Wide GPTM blocks
Watchdog Timer (WDT)	Two watchdog timers
Hibernation Module (HIB)	Low-power battery-backed Hibernation module
General-Purpose Input/Output (GPIO)	Six physical GPIO blocks
Advanced Motion Control	
Pulse Width Modulator (PWM)	Two PWM modules, each with four PWM generator blocks and a control block, for a total of 16 PWM outputs.
Quadrature Encoder Interface (QEI)	Two QEI modules
Analog Support	
Analog-to-Digital Converter (ADC)	Two 12-bit ADC modules with a maximum sample rate of one million samples/second
Analog Comparator Controller	Two independent integrated analog comparators
Digital Comparator	16 digital comparators
JTAG and Serial Wire Debug (SWD)	One JTAG module with integrated ARM SWD
Package	64-pin LQFP
Operating Range (Ambient)	Industrial (-40°C to 85°C) temperature range Extended (-40°C to 105°C) temperature range

Fig. 4.2. Table showing the features of TM4C123GH6PM Microcontroller

4.1.2.2 TM4C123GH6PM Microcontroller Pin Structure

Fig. 4.3 draws the I/O port structure for the TM4C123GH6PM. This microcontroller is used on the EK-TM4C123GXL Launchpad. [26] Pins on the LM3S family have two possibilities: digital I/O or an alternative function. However, pins on the TM4C family can be assigned to as many as eight different I/O functions. Pins can be configured for digital I/O, analog input, timer I/O, or serial I/O. For example PA0 can be digital I/O or serial input. There are two buses used for I/O. The digital I/O ports are

connected to both the advanced peripheral bus and the advanced high-performance bus. Because of the multiple buses, the microcontroller can perform I/O bus cycles simultaneous with instruction fetches from flash ROM. The TM4C123GH6PM has eight UART ports, four SSI ports, four I2C ports, two 12-bit ADCs, twelve timers, a CAN port, and a USB interface. The TM4C123GH6PM adds up to 16 PWM outputs. There are 43 I/O lines. There are twelve ADC inputs; each ADC can convert up to 1M samples per second.

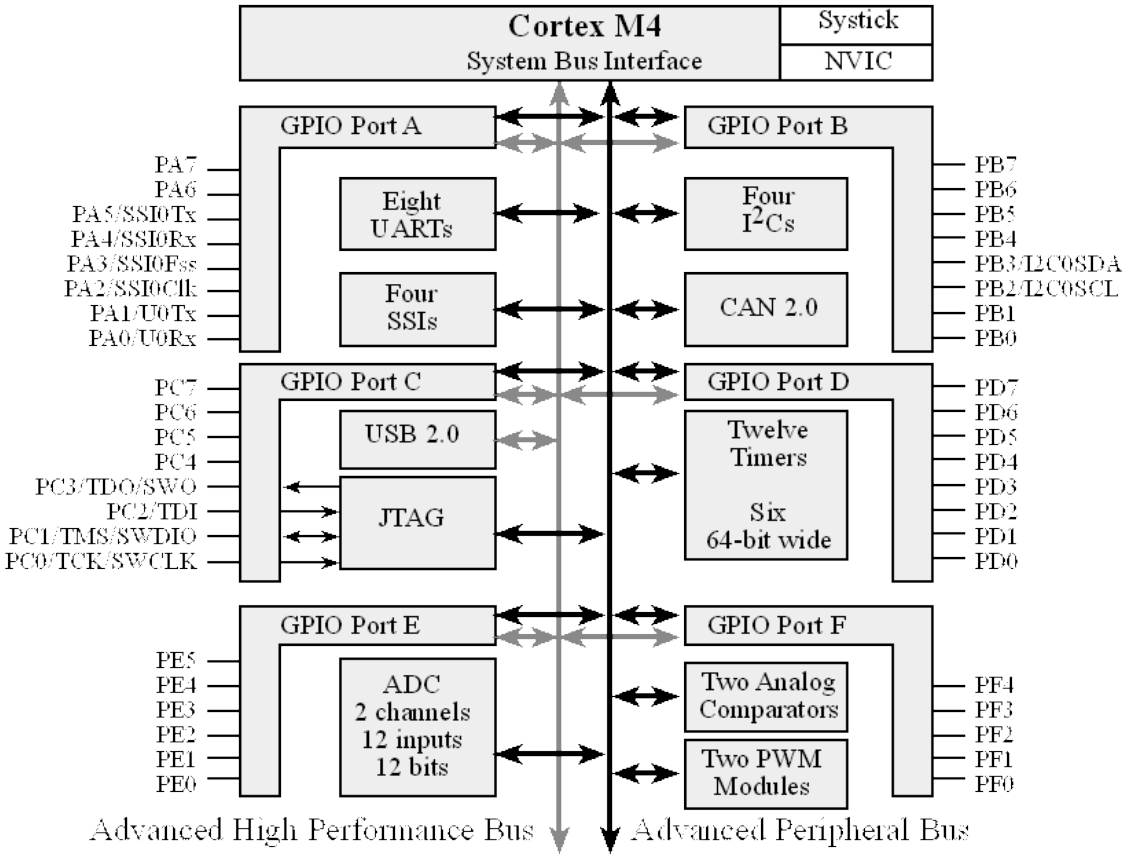

Fig. 4.3. I/O port pins for the TM4C123GH6PM microcontroller.

Each pin has one configuration bit in the GPIOAMSEL register. We set this bit to connect the port pin to the ADC or analog comparator. For digital functions, each pin also has four bits in the GPIOPCTL register, which we set to specify the alternative function for that pin (0 means regular I/O port). Not every pin can be connected to every alternative function.

Pins PC3 – PC0 were left off table in Fig. 4.2 because these four pins are reserved for the JTAG debugger and should not be used for regular I/O. Notice, most alternate function modules (e.g., U0Rx) only exist on one pin (PA0). While other functions could be mapped to two or three pins (e.g., CAN0Rx could be mapped to one of the following: PB4, PE4, or PF0.)

For example, if we wished to use UART7 on pins PE0 and PE1, we would set bits 1, 0 in the GPIO_PORTE_DEN_R register (enable digital), clear bits 1, 0 in the GPIO_PORTE_AMSEL_R register (disable analog), set the PMCx bits in the GPIO_PORTE_PCTL_R register for PE0, PE1 to 0001 (enable UART functionality),

and set bits 1, 0 in the GPIO_PORTE_AFSEL_R register (enable alternate function). If we wished to sample an analog signal on PD0, we would set bit 0 in the alternate function select register, clear bit 0 in the digital enable register (disable digital), set bit 0 in the analog mode select register (enable analog), and activate one of the ADCs to sample channel 7.

4.1.2.3 Tiva LaunchPad based on the TM4C123GH6PM

The LaunchPad evaluation board (Figure 4.4) is a low-cost development board available as part number EK-LM4F120XL and EK-TM4C123GXL. The microcontroller board provides an integrated In-Circuit Debug Interface (ICDI), which allows programming and debugging of the on board LM4F120 or TM4C123 microcontroller. [26] One USB cable is used by the debugger (ICDI), and the other USB allows the user to develop USB applications (device). The user can select board power to come from either the debugger (ICDI) or the USB device (device) by setting the Power selection switch.

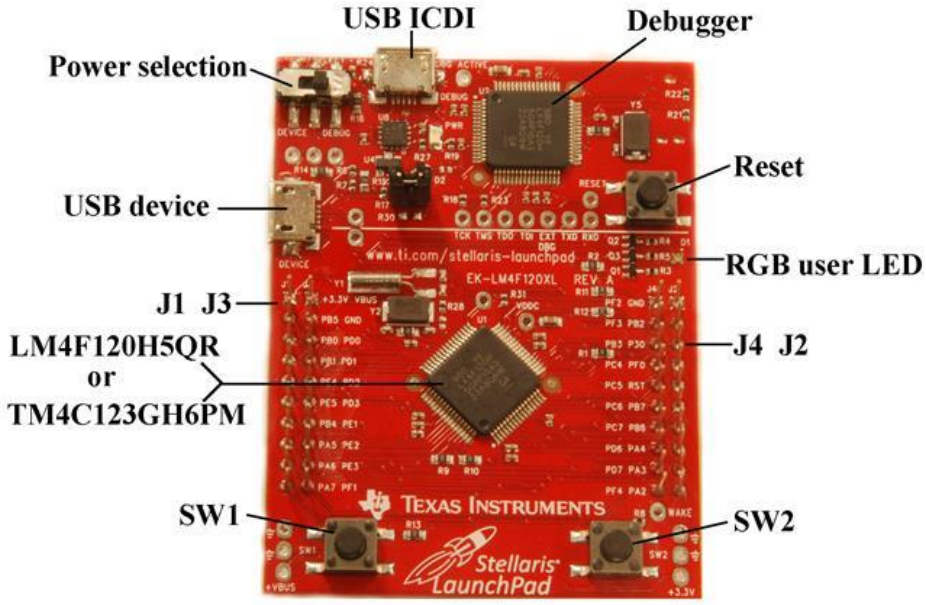

Fig. 4.4. Tiva LaunchPad based on the TM4C123GH6PM.

Pins PA1 – PA0 create a serial port, which is linked through the debugger cable to the PC. The serial link is a physical UART as seen by the LF4F120/TM4C and mapped to a virtual COM port on the PC. The USB device interface uses PD4 and PD5. The JTAG debugger requires pins PC3 – PC0. The LaunchPad connects PB6 to PD0, and PB7 to PD1. If you wish to use both PB6 and PD0 you will need to remove the R9 resistor. Similarly, to use both PB7 and PD1 remove the R10 resistor.

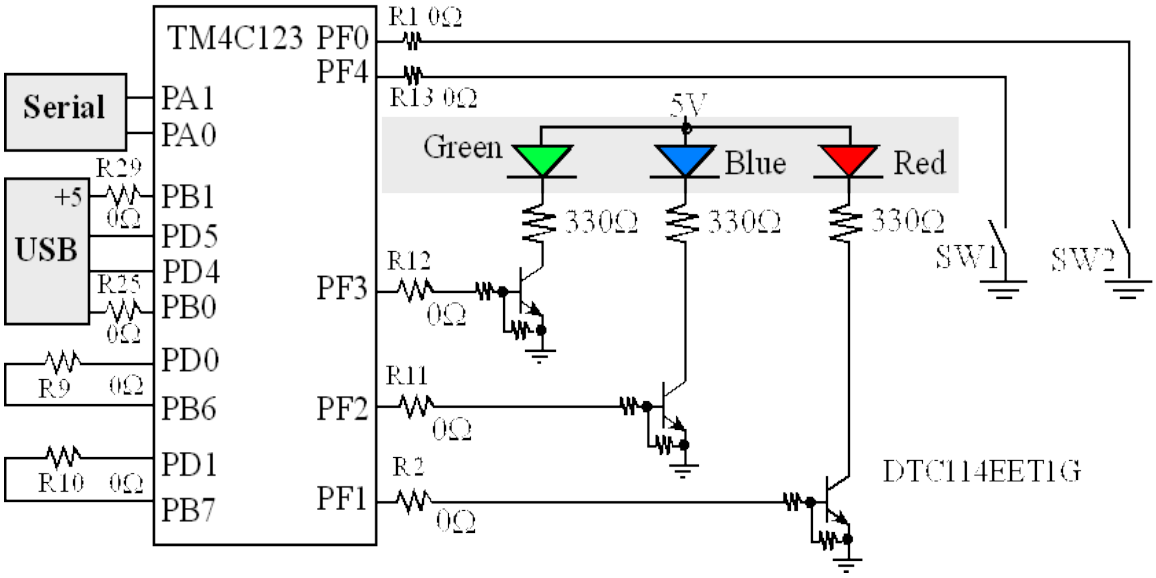

Fig. 4.5. Switch and LED interfaces on the Tiva LaunchPad Evaluation Board. The zero ohm resistors can be removed so the corresponding pin can be used for its regular purpose.

The Tiva LaunchPad evaluation board has two switches and one 3-color LED. See Fig. 4.5. The switches are negative logic and will require activation of the internal pull-up resistors. In particular, you will set bits 0 and 4 in GPIO_PORTF_PUR_R register. The LED interfaces on PF3 – PF1 are positive logic. To use the LED, make the PF3 – PF1 pins an output. To activate the red colour, output a one to PF1. The blue colour is on PF2, and the green colour is controlled by PF3. The 0-Ω resistors (R1, R2, R11, R12, R13, R25, and R29) can be removed to disconnect the corresponding pin from the external hardware.

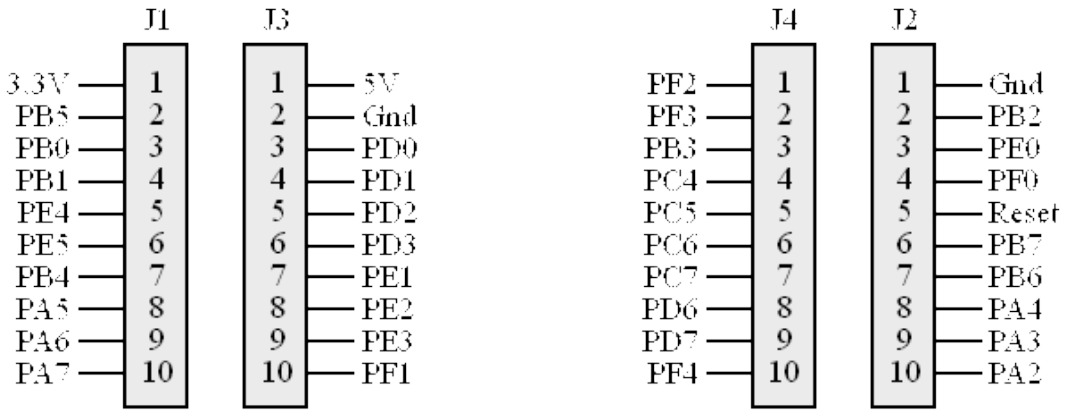

Fig. 4.6. Interface connectors on the Tiva TM4C123 LaunchPad Evaluation Board.

The LaunchPad has four 10-pin connectors, labelled as J1 J2 J3 J4 in Fig. 18 and Fig. 4.6, to which you can attach your external signals. The top side of these connectors has male pins, and the bottom side has female sockets. The intent is to stack boards together to make a layered system. Texas Instruments also supplies Booster Packs, which are pre-made external devices that will plug into this 40-pin connector. The Booster Packs for the MSP430 LaunchPad are compatible with this board. One simply plugs the 20-pin connectors of the MSP430 booster into the outer two rows. The inner 10-pin headers (connectors J3 and J4) apply only to Stellaris or Tiva Booster Packs.

4.1.3 LM2596 DC-DC Step-Down Buck Converter

The LM2596 DC-DC Buck converter is used to take an input voltage of 4.5V to 35V to produce an output voltage ranging from 1.23V to 30V. The voltage at the output end is adjusted using the potentiometer screw [see Fig. 4.7 (a)], present at the top of the blue box. The circuit diagram for the buck boost is shown is Fig. 4.7 (b).

(a)

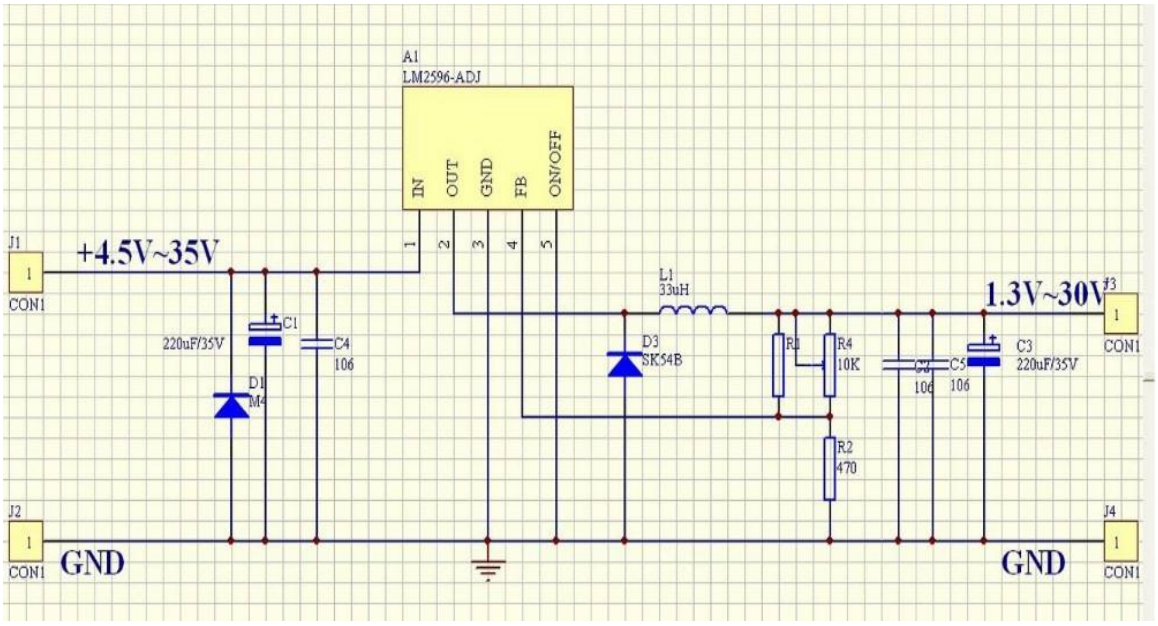

Fig. 4.7. (a) LM2596 DC-DC Step Down Buck Converter. (b) Schematic diagram for LM2596 DC-DC Step Down Buck Converter.

The buck boost is used to step down the 11.1V from the Li-ion battery module, to produce a voltage of 9.5V to be supplied to the gripper circuit. The specification of the buck boost are given in the table below [27].

Basic Attributes

Module Property	**Non-isolation buck**	**Rectification mode**	**Synchronous rectifier**
Input voltage	4V-35V	Output Voltage	1.23V-30V
Input current	3A (maximum)	Conversion efficiency	92% (highest)
Switching frequency	150KHz	Output ripple	30mV (maximum)
Load regulation	± 0.5%	Voltage regulation	± 2.5%
Work temperature	-40 - +85	Overall dimension	48*23*14(L*W*H)(mm)

4.2 Software Specifications

The project required the use of three softwares in all for development of a working prototype of the robotic gripper using NiTi coils. The softwares were used for designing, fabrication and developing a control circuit for the gripper. The following softwares were used:

- SolidWorks® 3D Cad Software
- Cura 3D Printing Slicing Software
- µVision® IDE (Integrated Development Environment) from Keil Software

SolidWorks was used for designing of the finger links and the base of the gripper, and has been discussed in section 3.3. The software Cura was used during fabrication of the links and the base of gripper through the 3D printer. The µVision® IDE combines project management, run-time environment, build facilities, source code editing, and program debugging in a single powerful environment. It is for programming of the microcontroller discussed in section 4.1.2.

4.2.1 Code for the microcontroller

```
#include "tm4c123gh6pm.h"
#include "Port_Init.h"
// ***** 2. Global Declarations Section *****
#define SYSCTL_RCGC2_R          (*((volatile unsigned long *)0x400FE108))
#define GPIO_PORTE_DATA_R       (*((volatile unsigned long *)0x400243FC))
#define GPIO_PORTE_DIR_R        (*((volatile unsigned long *)0x40024400))
#define GPIO_PORTE_AFSEL_R      (*((volatile unsigned long *)0x40024420))
#define GPIO_PORTE_DEN_R        (*((volatile unsigned long *)0x4002451C))
#define GPIO_PORTE_AMSEL_R      (*((volatile unsigned long *)0x40024528))
#define GPIO_PORTE_PCTL_R       (*((volatile unsigned long *)0x4002452C))
#define GPIO_PORTF_DATA_R       (*((volatile unsigned long *)0x400253FC))
#define GPIO_PORTF_DIR_R        (*((volatile unsigned long *)0x40025400))
#define GPIO_PORTF_AFSEL_R      (*((volatile unsigned long *)0x40025420))
#define GPIO_PORTF_PUR_R        (*((volatile unsigned long *)0x40025510))
#define GPIO_PORTF_DEN_R        (*((volatile unsigned long *)0x4002551C))
#define GPIO_PORTF_LOCK_R       (*((volatile unsigned long *)0x40025520))
#define GPIO_PORTF_CR_R         (*((volatile unsigned long *)0x40025524))
#define GPIO_PORTF_AMSEL_R      (*((volatile unsigned long *)0x40025528))
#define GPIO_PORTF_PCTL_R       (*((volatile unsigned long *)0x4002552C))
#define SYSCTL_RCGC2_R          (*((volatile unsigned long *)0x400FE108))
unsigned long in;
// FUNCTION PROTOTYPES: Each subroutine defined
void DisableInterrupts(void); // Disable interrupts
void EnableInterrupts(void);  // Enable interrupts
void delayms(unsigned long);// Delay function
// ***** 3. Subroutines Section *****
void PortE_Init(){volatile unsigned long delay;
       SYSCTL_RCGC2_R |= 0x00000010;
       delay = SYSCTL_RCGC2_R;
       GPIO_PORTE_DIR_R |= 0x06;
       GPIO_PORTE_AFSEL_R &= ~0x06;
       GPIO_PORTE_AMSEL_R &= ~0x06;
       GPIO_PORTE_PCTL_R &= ~0x00000FF0;
       GPIO_PORTE_DEN_R |= 0x06;
}
```

```
void PortF_Init(){volatile unsigned long delay;

       SYSCTL_RCGC2_R |= 0x00000020;

       delay = SYSCTL_RCGC2_R;

       GPIO_PORTF_LOCK_R = 0x4C4F434B;

       GPIO_PORTF_CR_R = 0x11;

       GPIO_PORTF_DIR_R &= ~0x11;

       GPIO_PORTF_AMSEL_R &= ~0x11;

       GPIO_PORTF_AFSEL_R &= ~0x11;

       GPIO_PORTF_DEN_R |= 0x11;

       GPIO_PORTF_PCTL_R &= ~0x0000000F;

       GPIO_PORTF_PUR_R |= 0x11;

int main(void){

  unsigned long volatile delay;

       TExaS_Init(SW_PIN_PE0, LED_PIN_PE1);  // Set system clock to 80 MHz

       PortE_Init();       // Initialising PE1 and PE2 on PortE
       PortF_Init();      // Initialising the two switches on PortF
       while(1){
              if(GPIO_PORTF_DATA_R == 0x01){          // check if switch 1 pressed
                     while(GPIO_PORTF_DATA_R == 0x01)
                            GPIO_PORTE_DATA_R |= 0x02;       // Opening Port E1
                     GPIO_PORTE_DATA_R &= ~0x02;             // Closing Port E1
                     delayms(3000);                    // Cooling deformation delay
              }
              else if(GPIO_PORTF_DATA_R == 0x10){     // check if switch 2 pressed
                     GPIO_PORTE_DATA_R |= 0x04;       // Enable Port E pin2
                     delayms(2000);                    // delay for 2 seconds

                     GPIO_PORTE_DATA_R &= ~0x04;      // Closing Port E pin2
                     delayms(3000);                    // Cooling deformation delay
              }
              else{
                     GPIO_PORTE_DATA_R &= ~0x06;
                                                 // Close PE1 and PE2 otherwise
              }
       }
 }
```

```
void delayms(unsigned long ms){
       unsigned long count;
  while(ms > 0 ) { // repeat while there are still ms to delay
    count = 16000; // number of counts to delay 1ms at 80MHz
    while (count > 0) {
      count--;
    } // This while loop takes approximately 3 cycles
ms--;
}
}
```

4.3 Control Circuit for the Gripper

A control circuit is required to control the grasp and release motion of the robotic gripper. The control circuit basically controls the current through the NiTi coils, hence controlling its actuation. Fig. 4.8 represents the control circuit for the robotic gripper.

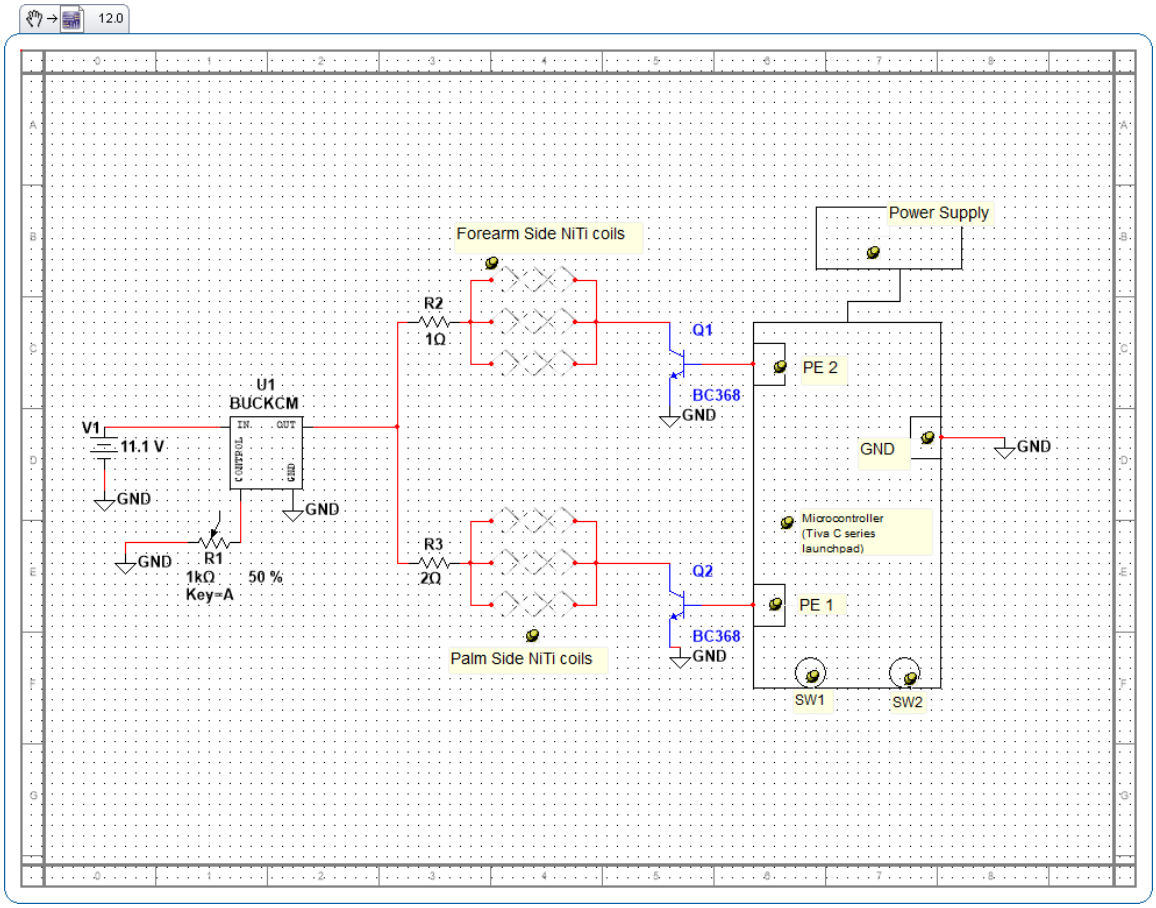

Fig. 4.8. Control circuit for the robotic gripper

[See Fig. 4.8] The control circuit consists of an 11.1 V Li-ion battery module represented by V1. It is further connected to a buck converter (represented as U1), which has an adjustable potentiometer (represented as R1). The value of R1 is adjusted so that the buck converter supplies a voltage of 9.5 V. The output of the buck converter is connected to R2 and R3, which in turn are connected in parallel. R2 is connected to the NiTi coils on the forearm side of the gripper, while R3 is connected to the palm side of the gripper. The NiTi coils on each side of the two resistors are connected in parallel to each other.

The NiTi coils on forearm side and palm side are further connected to the collector of the NPN transistors Q1 and Q2 respectively. The emitter end of the two transistors are connected to ground. The base of the two transistors Q1 and Q2 are connected to Port E pin1 and Port E pin2 of the microcontroller respectively. The switches SW1 and SW2 represent the Port F pin0 and Port F pin4 respectively of the microcontroller. These are tactile switches are embedded on the LaunchPad itself. The values of R2 and R3 are selected such that when the NiTi coils are actuated, a current of approximately 0.7 A runs through them. The GND pin on the microcontroller provides the ground terminal to the circuit.

Chapter 5.
WORKING OF THE PROJECT

5.1 Analogy between the Gripping by Human Hand and the Robotic Gripper

The hand has a very delicate and complex structure. This allows muscles and joints in the hand a great range of movement and precision. The different forces are also distributed in the hand in the best possible way. But the hand is also quite vulnerable: tendons, nerve fibers, blood vessels and very thin bones are all positioned right under the skin and are only protected by a thin layer of muscle and fat. Only the palm is protected by a strong pad of tendons (aponeurosis) for a powerful grip.

To grasp and move objects, the hand has two different ways of gripping things:

- Power grip
- Precision grip.

The technique used depends on whether the object is very large and very heavy, and what sort of shape it has and how easy it is to handle. The power grip is better suited for large, heavy objects, and the precision grip is used for small, lighter objects.

5.1.1 Power Grip

[22] The power grip is used for carrying heavy bags or for holding on to a handle, for example. In the power grip, the object is held in the palm of the hand, the long flexor tendons pull the fingers and the thumb so that they can tightly close around the object. This grip is made possible by the four other fingers flexing and, more importantly, the ability of the thumb to be positioned opposite the fingers. With the hand in this position, larger objects such as a stone or a heavy bottle can be held and moved in a controlled way. The greater the weight and the smoother the surface is, the more strength is needed for holding and moving the object.

The robotic gripper also uses the same technique for gripping of larger objects. The palm of the hand is represented by the base of the gripper and the tendons represent the NiTi coils. Since the robotic gripper is a three finger gripper, hence during the grasp motion, the two fingers flex together with the third finger acting as the thumb, situated opposite to the two fingers help in gripping an object similar to the human hand.

5.1.2 Precision Grip

The precision grip is important for delicately handling and moving an object, for example when writing, sewing or drawing. When using the precision grip, the thumb and the index finger work like a forceps: The thumb is opposite one or more fingertips, allowing the hand a controlled grip of even very small objects like a pencil or fine instruments. Depending on the weight of the object and the direction and speed of the movement, the brain directs the use of force and coordinates the muscles of the hand.

Although the current control circuit of the robotic gripper does not allow for precision grip but it can be modified to provide the functionality of precision grip to the robotic gripper. Such a control circuit would require to actuate each finger independently and hence the combination of any two can be used to provide precision grip.

5.2 Implementation of the Robotic Gripper

The control circuit [See Fig. 4.8] is designed in a way such that the gripper can perform grasp and release motion. With the current control circuit, the gripper can only perform a power grip. The grasp and release motion performed by the gripper is controlled using the two switches SW1 and SW2, embedded on the microcontroller [See Fig. 5.1]. The Fig. 5.1 (a), represents the control circuit during grasp motion of the microcontroller. The functionality of the griper is such that as long as the SW1 on the microcontroller is pressed Port E pin 1 is open and a current flows through it.

This in turn activates the base of the NPN transistor Q2 and the collector and emitter of Q2 get electrically connected. As a result the NiTi coils on the palm side of the gripper get connected to the ground and a current flows through them. A current of 0.7A flows through each finger of the gripper and a result the NiTi coils get actuated and gets transformed to their austenite phase. As a result the finger links flexes towards each other, which in turn results in the gripping action of the robotic gripper. It should be noted that switch SW1 should be pressed for at least two seconds for the gripper to perform the gripping action. This is because the NiTi coils require a current of 0.7A for at least two seconds for complete phase transformation.

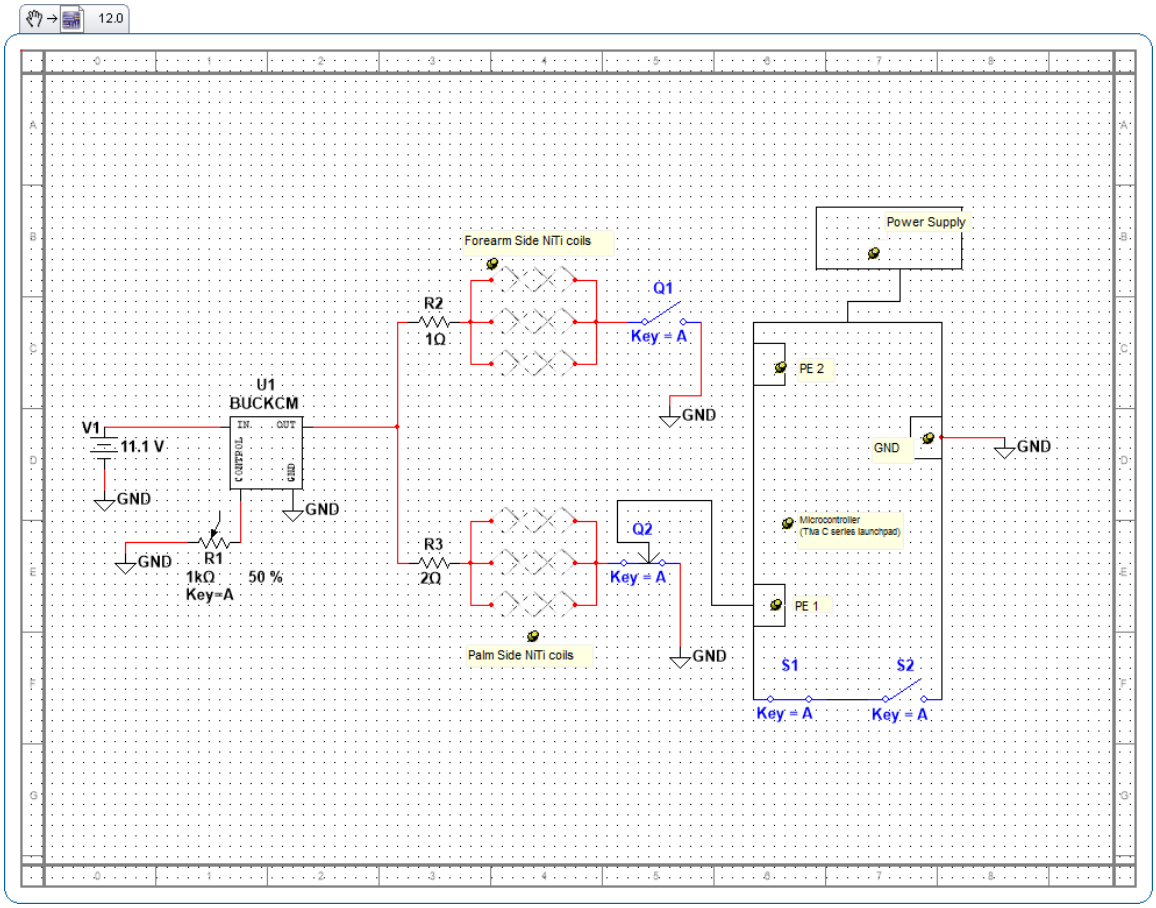

(a)

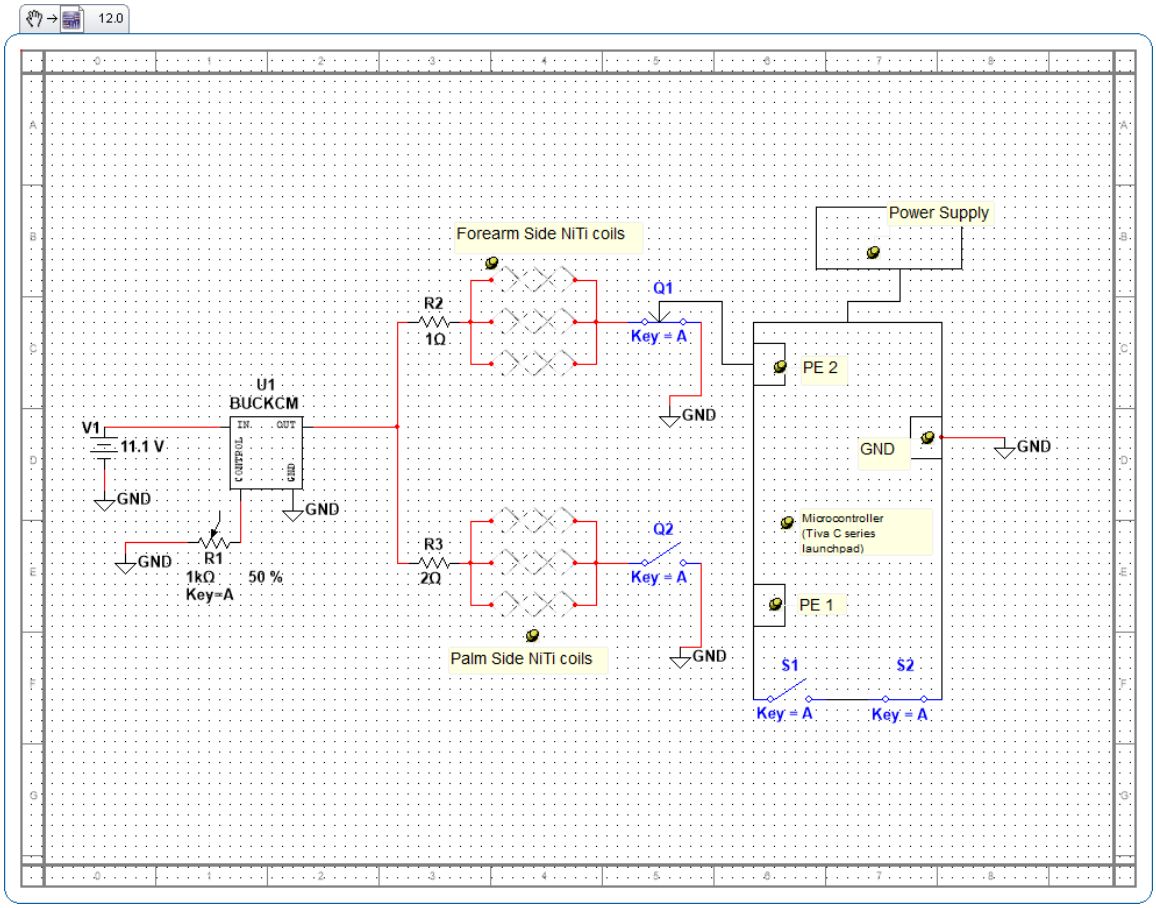

(b)

Fig. 5.1. (a) Control circuit during grasp action of the robotic gripper. (b) Control circuit during the release action of the robotic gripper

Similarly, when switch SW2 on the microcontroller is pressed, Port E pin 2 is opened [See Fig. 5.1 (b)] for a period of two seconds. This in turn activates the base of transistor Q1 and its collector gets connected to its emitter. Hence the NiTi coils on the forearm side are connected to ground. This in turn circulates a current of 0.7A in each finger (on the forearm side) of the gripper. This result in flexing of the links away from each other and the gripper performs the release action.

Since the Port E pin 2 was opened only for two seconds, hence the current in the coils also flows only for two seconds. This time is enough for the gripper to perform the release action and as well as prevents the NiTi coils from excessive heat produced by the current. There is also a three second delay after every grasp or release action of the gripper. This is because it takes about three seconds for the NiTi coils to cool down from its austenite to martensite phase after the current is removed. During the cooling deformation period of three seconds, neither of the switches are operational. This helps in preventing any permanent deformation in the NiTi coils.

Chapter 6.
RESULTS AND DISCUSSION

The Robotic gripper is fixed to a wooden arm through the hole present at back of the base of the gripper. The control circuit along with the microcontroller and the battery is connected to the wooden arm. The robotic gripper uses an open loop control to perform the grasp and release motion. When SW1 on the microcontroller is pressed the robotic gripper grasps the object. When SW2 on the microcontroller is pressed the robotic gripper releases the object. Fig.6.1 shows the gripping and release of an object by the robotic gripper.

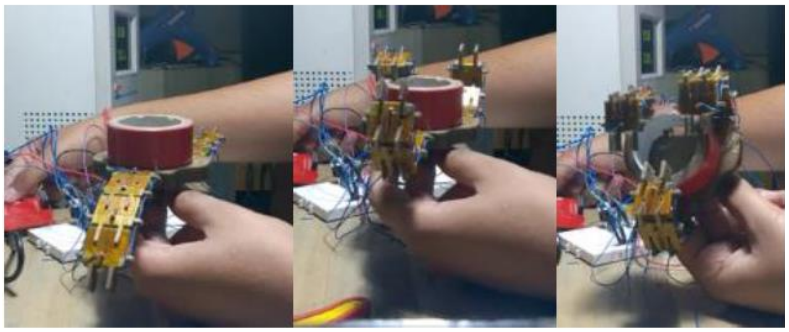

(a) (b) (c)

Fig.6.1. Gripper during the gripping of an object. (a) Gripper at rest. (b) Movement of fingers during gripping. (c) Full grip of the object.

6.1 Advantages of the Developed System

The use of NiTi coils as actuators provide better mechanical performance. Flexinol® actuator wires are smaller by far than alternatives. At least 1,000 times smaller than solenoids for the same work done. Due to their small size, they make the gripper very light in weight. Flexinol® actuator springs can be used as it is, thus eliminating gear boxes, housings, bearings, and so on. Their flexible forgiving performance is easier to work with. Thus the robotic gripper has a simple circuit that can be easily modified. In corrosive environments Flexinol® actuator wires' high corrosion resistance really pays off. Flexinol® actuator wires are inexpensive to buy and cost less and therefore helps in manufacturing a cheap robotic gripper.

Using a Three Finger Gripper provides a greater flexibility and more reliability to grip or grasp different kinds of parts. Since NiTi coils undergo a structural phase transformation when actuated, hence the robotic gripper provides a strong power grip till the switch is pressed. The NiTi coils have a lifetime of about million cycles, hence can be used for a long time. They doesn't require any maintenance once installed, hence thus reduces the maintenance cost. Since the NiTi coils are attached only through a screw to the finger links, hence can be easily replaced when damaged. Since the fingers of the gripper are electrically connected in parallel [See Fig. 5.1], hence additional fingers can be added without altering the control circuit. The only modification required would be in the model of the base of the gripper where the fingers are finally attached.

6.2 Limitations

NiTi have many advantages over traditional actuators, but do suffer from a series of limitations that may impede practical application.

- **Response time and response symmetry**: SMA actuators are typically actuated electrically, where an electric current results in Joule heating. Deactivation typically occurs by free convective heat transfer to the ambient environment. Consequently, SMA actuation is typically asymmetric, with a relatively fast actuation time and a slow deactuation time.
  A number of methods have been proposed to reduce SMA deactivation time, including forced convection, [15] and lagging the SMA with a conductive material in order to manipulate the heat transfer rate.

  Novel methods to enhance the feasibility of SMA actuators include the use of a conductive "lagging". This method uses a thermal paste to rapidly transfer heat from the SMA by conduction. This heat is then more readily transferred to the environment by convection as the outer radii (and heat transfer area) is significantly greater than for the bare wire. This method results in a significant reduction in deactivation time and a symmetric activation profile. As a consequence of the increased heat transfer rate, the required current to achieve a given actuation force is increased. [16]

- **Structural fatigue and functional fatigue:** NiTi is subject to structural fatigue – a failure mode by which cyclic loading results in the initiation and propagation of a crack that eventually results in catastrophic loss of function by fracture. The physics behind this fatigue mode is accumulation of microstructural damage during cyclic loading. This failure mode is observed in most engineering materials, not just SMAs.
  NiTi coils are also subject to functional fatigue, a failure mode not typical of most engineering materials, whereby the SMA does not fail structurally but loses its Shape memory characteristics over time. As a result of cyclic loading (both mechanical and thermal), the material loses its ability to undergo a reversible phase transformation. For example, the working displacement in an actuator decreases with increasing cycle numbers. The physics behind this is gradual change in microstructure—more specifically, the build-up of accommodation slip dislocations. This is often accompanied by a significant change in transformation temperatures. [18]

- **Unintentional Actuation:** NiTi actuators are typically actuated electrically by Joule heating. If the NiTi is used in an environment where the ambient temperature is uncontrolled, unintentional actuation by ambient heating may occur.

Chapter 7.
CONCLUSION AND FUTURE SCOPE

7.1 Conclusion

This report demonstrated a Soft Robotic Gripper using NiTi coils as the actuators. The development, modelling and fabrication of NiTi coil actuators has been discussed. The report well informs about the modelling and fabrication of the links of the finger and the base of the gripper, construction of the fingers using these links and assembling of the gripper as a whole. The control circuit used to control the grasp and release motion of the gripper has been briefly discussed.

A detailed overview of the components and the software used in the process have also been discussed. The phase transformation property of the NiTi coils when current is supplied to them, is used to produce the grasp and release movement of the links of the finger. The current control circuit of the gripper is designed only for power gripping. The circuit can be modified to produce a precision grip.

The control circuit consists of a microcontroller that control the actuation of the NiTi coils. The two switches on the on the microcontroller are used to perform the grasp and release action of the gripper. The whole setup is attached to wooden arm to provide a firm for the control circuit and hold the gripper during the grasp and release motion.

7.2 Future Scope

The three fingers robotic gripper can be extended to a full five finger gripper and thus could replicate all the gestures performed by the human hand. This will also provide a much firmer grip on the object it grasps. The control circuit of the gripper can also be modified to produce precision grip, similar to that of the human hand. The design of the robotic gripper could be modified to design limbs of other animals.

The technology used in the gripper, can be applied to a glove, which in turn could be used to provide movement to the hands of a paralysed person. Similarly, it can be used to develop other wearables. The gripper can also be used to interface with the robotic arms used in industrial automation as means for a cheaper and better gripper.

The robotic gripper can also be used to sync with a brain control interface and thus one could control the gripper through his mind. The technology used to develop the robotic gripper can also be used to develop a robotic arm and other parts of the body.

REFERENCES

1. Monkman, G. J.; Hesse, S.; Steinmann, R.; Schunk, H. (2007). Robot Grippers. WileyVCH.p. 62. ISBN 9783527406197.
2. Fantoni, G., Santochi, M., Dini, G., Tracht, K., ScholzReiter,B., Fleischer, J., Lien, T.K., Seliger, G.,Reinhart, G.,Franke, J., Hansen, H.N., Verl, A.,2014, Grasping devices and methods in automated production processes, CIRP Annals Manufacturing Technology, Volume 63, Issue 2, 2014, Pages 679701, ISSN 00078506, http://dx.doi.org/10.1016/j.cirp.2014.05.006.
3. Biologically Inspired Robotics Wikipedia
4. Trivedi, D., Rahn, C. D., Kier, W. M., & Walker, I. D. (2008). Soft robotics: Biological inspiration, state of the art, and future research. Applied Bionics and Biomechanics, 5(3), 99117.
5. R. Shepherd, F. Ilievski, W. Choi, S. Morin, A. Stokes, A. Mazzeo, X. Chen, M. Wang, and G. Whitesides, "Multigait soft robot," Proceedings of the National Academy of Sciences, vol. 108, no. 51, pp. 20400–20403, 2011.
6. "Robotics Grasping and Force closure" (PDF). pdf. FU Berlin. Retrieved 20140320.
7. Micro artificial muscle fiber using NiTi spring for soft robotics Sangbae Kim, Elliot Hawkes, Kyujin Choy, Matthew Joldaz, Joe Foleyz and Robert Wood Harvard Micro robotics Laboratory Harvard University, Cambridge, Massachusetts, Seoul National University Seoul, South Korea Government & Industrial Research iRobot Corporation Bedford, Massachusetts.
8. Bi-Chiau Chang, John Shaw, and Mark Iadicola. Thermodynamics of shape memory alloy wire: Modelling, experiments, and application. Continuum Mechanics and Thermodynamics, 18(1):83–118, 2006.
9. B. Kim, M.G. Lee, Y.P. Lee, Y. Kim, and G. Lee. An earthworm-like micro robot using shape memory alloy actuator. Sensors and Actuators, A: Physical, 125(2):429–437, 2006.
10. Hyo Jik Lee and Jung Ju Lee. Evaluation of the characteristics of a shape memory alloy spring actuator. Smart Materials and Structures, 9(6):817–823, 2000.
11. Y. Dong, Z. Boming, and L. Jun. A changeable aerofoil actuated by shape memory alloy springs. Materials Science and Engineering A, 485(1-2):243–250, 2008.
12. K.J. Cho, E. Hawkes, C. Quinn, and R.J. Wood. Design, fabrication and analysis of a body-caudal fin propulsion system for a micro robotic fish. In Proceedings - IEEE International Conference on Robotics and Automation, pages 706–711, 2008.
13. Tom C. Waram. Actuator Design Using Shape Memory Alloys. T.C. Waram, 1063 King St. W., Suite 204 Hamilton, Ontario L8S 1L8 Canada, second edition, 1993. Phone: (905)525-8251.
14. M. Dolce and D. Cardone, "Mechanical behaviour of shape memory alloys for seismic applications—1. Martensite and austenite NiTi bars subjected to torsion," Int. J. Mech. Sci., vol. 43, pp. 2631–2656, Nov. 2001.
15. B. Chang, J. Shaw, and M. Iadicola, "Thermodynamics of shape memory alloy wire: Modelling, experiments, and application," Continuum Mech. Thermodyn., vol. 18, no. 1, pp. 83–118, 2006.

16. Meshworm: A Peristaltic Soft Robot With Antagonistic Nickel Titanium Coil Actuators Sangok Seok, Cagdas Denizel Onal, Member, IEEE, Kyu-Jin Cho, Member, IEEE, Robert J. Wood, Daniela Rus, Fellow, IEEE, and Sangbae Kim.
17. Y. Liu, “Detwinning process and its anisotropy in shape memory alloys,” Proc. SPIE Smart Mater., vol. 4234, pp. 82–93, 2001.
18. K. Otsuka and C. M. Wayman, Shape Memory Materials. Cambridge, U.K.: Cambridge Univ. Press, 1998.
19. Technical data sheet of Flexinol, Dynalloy, Inc. makers of dynamic alloys.
20. HeathPages.org,http://www.healthpages.org/anatomyfunction/anatomyhandwrist/
21. Schmidt R, Lang F, Heckmann M. Physiologie des Menschen: mit Pathophysiologie. Heidelberg: Springer. 2011.
22. National Library of Medicine PubMed Health, http://www.ncbi.nlm.nih.gov/pubmedhealth/PMH0072546/
23. PLA RepRapWiki, http://reprap.org/wiki/PLA
24. BC368 NPN General Purpose Amplifier, Technical Datasheet, Fairchild Semiconductors.
25. Tiva™ TM4C123GH6PM Microcontroller Datasheet, Texas Instruments
26. Chapter 6: Parallel I/O, ports Embedded Systems: Introduction to ARM Cortex-M Microcontrollers, Jonathan Valvano and Ramesh Yerraballi, 2014, ISBN: 978-1477508992, http://users.ece.utexas.edu/~valvano/arm/outline1.htm
27. LM2596 DC-DC Step-Down Buck Converter Datasheet.